

Institutionen för systemteknik

Department of Electrical Engineering

Examensarbete

Sensor Fusion for Enhanced Lane Departure Warning System

Examensarbete utfört i Reglerteknik
vid Tekniska högskolan i Linköping
av

Erik Almgren

LITH-ISY-EX--06/3829--SE

Linköping 2006



Linköpings universitet
TEKNISKA HÖGSKOLAN

Department of Electrical Engineering
Linköpings universitet
SE-581 83 Linköping, Sweden

Linköpings tekniska högskola
Linköpings universitet
581 83 Linköping

Sensor Fusion for Enhanced Lane Departure Warning System

Examensarbete utfört i Reglerteknik
vid Tekniska högskolan i Linköping
av


Erik Almgren

LITH-ISY-EX--06/3829--SE

Handledare: **Stefan Johansson**
Autoliv Electronics
Jeroen Hol
ISY, Linköpings universitet

Examinator: **Dr. Rickard Karlsson**
ISY, Linköpings universitet

Linköping, 12 October, 2006

	Avdelning, Institution Division, Department Division of Automatic Control Department of Electrical Engineering Linköpings universitet S-581 83 Linköping, Sweden	Datum Date 2006-10-12						
Språk Language <input type="checkbox"/> Svenska/Swedish <input checked="" type="checkbox"/> Engelska/English <input type="checkbox"/> _____	Rapporttyp Report category <input type="checkbox"/> Licentiatavhandling <input checked="" type="checkbox"/> Examensarbete <input type="checkbox"/> C-uppsats <input type="checkbox"/> D-uppsats <input type="checkbox"/> Övrig rapport <input type="checkbox"/> _____	ISBN _____ ISRN LITH-ISY-EX--06/3829--SE Serietitel och serienummer ISSN Title of series, numbering _____						
URL för elektronisk version http://www.control.isy.liu.se http://www.ep.liu.se/2006/3829								
<table border="0"> <tr> <td style="vertical-align: top;">Titel Title</td> <td>Sensorfusion för förbättrad filavvikelsevarning Sensor Fusion for Enhanced Lane Departure Warning System</td> </tr> <tr> <td colspan="2"> </td> </tr> <tr> <td style="vertical-align: top;">Författare Author</td> <td>Erik Almgren</td> </tr> </table>			Titel Title	Sensorfusion för förbättrad filavvikelsevarning Sensor Fusion for Enhanced Lane Departure Warning System	 		Författare Author	Erik Almgren
Titel Title	Sensorfusion för förbättrad filavvikelsevarning Sensor Fusion for Enhanced Lane Departure Warning System							
Författare Author	Erik Almgren							
Sammanfattning Abstract <p>A lane departure warning system relying exclusively on a camera has several shortcomings and tends to be sensitive to, e.g., bad weather and abrupt manoeuvres. To handle these situations, the system proposed in this thesis uses a dynamic model of the vehicle and integration of relative motion sensors to estimate the vehicle's position on the road. The relative motion is measured using vision, inertial, and vehicle sensors. All these sensors types are affected by errors such as offset, drift and quantization. However the different sensors are sensitive to different types of errors, e.g., the camera system is rather poor at detecting rapid lateral movements, a type of situation which an inertial sensor practically never fails to detect. These kinds of complementary properties make sensor fusion interesting. The approach of this Master's thesis is to use an already existing lane departure warning system as vision sensor in combination with an inertial measurement unit to produce a system that is robust and can achieve good warnings if an unintentional lane departure is about to occur. For the combination of sensor data, different sensor fusion models have been proposed and evaluated on experimental data. The models are based on a nonlinear model that is linearized so that a Kalman filter can be applied. Experiments show that the proposed solutions succeed at handling situations where a system relying solely on a camera would have problems. The results from the testing show that the original lane departure warning system, which is a single camera system, is outperformed by the suggested system.</p>								
Nyckelord Keywords CUSUM-test, Extended Kalman Filter, Kalman Filter, Lane Departure Warning System, Sensor Fusion, Monte Carlo Simulations, Vehicle Dynamics								

Abstract

A lane departure warning system relying exclusively on a camera has several shortcomings and tends to be sensitive to, e.g., bad weather and abrupt manoeuvres. To handle these situations, the system proposed in this thesis uses a dynamic model of the vehicle and integration of relative motion sensors to estimate the vehicle's position on the road. The relative motion is measured using vision, inertial, and vehicle sensors. All these sensors types are affected by errors such as offset, drift and quantization. However the different sensors are sensitive to different types of errors, e.g., the camera system is rather poor at detecting rapid lateral movements, a type of situation which an inertial sensor practically never fails to detect. These kinds of complementary properties make sensor fusion interesting. The approach of this Master's thesis is to use an already existing lane departure warning system as vision sensor in combination with an inertial measurement unit to produce a system that is robust and can achieve good warnings if an unintentional lane departure is about to occur. For the combination of sensor data, different sensor fusion models have been proposed and evaluated on experimental data. The models are based on a nonlinear model that is linearized so that a Kalman filter can be applied. Experiments show that the proposed solutions succeed at handling situations where a system relying solely on a camera would have problems. The results from the testing show that the original lane departure warning system, which is a single camera system, is outperformed by the suggested system.

Acknowledgements

First of all I would like to thank my supervisor at Autoliv Electronics, Stefan Johansson. Stefan has provided help and support with theoretical and practical problems that have arisen during the project. Salah Hadi is gratefully acknowledged for his great management and support. I would also like to thank Dr. Rickard Karlsson for his valuable comments and suggestions. Special thanks to my supervisor at LiTH, Jeroen Hol for his feedback. Elisabeth Ågren deserves extra gratitude for all her help. Finally I would like to thank Erik Gudmundson, Peter Juhlin-Dannfelt and Per Löfgren for proof-reading.

Linköping, Oktober 2006
Erik Almgren

Contents

1	Introduction	1
1.1	Background	1
1.1.1	Accident Types	1
1.1.2	Sensor Fusion	2
1.1.3	Autoliv Electronics	3
1.2	Problem Definition	3
1.3	Objectives	3
1.4	Limitations	4
1.5	Outline	4
2	Sensor Fusion Techniques	5
2.1	Advantages of Sensor Fusion	5
2.2	Bayesian Estimation	6
2.2.1	The Kalman Filter	7
2.2.2	The Extended Kalman Filter	8
2.2.3	Sampling of a Continues Time System	9
3	Vehicle and Sensor Models	11
3.1	Coordinate Systems	11
3.1.1	Vehicle Coordinates	11
3.1.2	Sensor Coordinates	11
3.2	Process Model	13
3.2.1	Movement in Vehicle Coordinates	13
3.2.2	The Bicycle Model	14
3.2.3	Road Model	17
3.2.4	Heading Angle	18
3.2.5	Lateral Position on the Road	18
3.2.6	Process Model - Summary	19
3.2.7	Process Noise - Piecewise Constant Acceleration	20
3.3	Measurement Model	22
3.3.1	Road Vehicle Geometry	22
3.3.2	Yaw Rate and Lateral Acceleration	22
3.3.3	Lateral Offset	23
3.3.4	Lane Width	26

3.3.5	Road Curvature	26
3.3.6	Vehicle Speed and Wheel Turn Angle	26
3.3.7	Measurement Model - Summary	26
4	Decision Strategies	29
4.1	Time to Lane Crossing	29
4.2	CUSUM-test for Detecting Lane Departure	29
5	Filter Evaluation	33
5.1	Monte Carlo Simulations	33
5.2	Simulation Input Signals	34
5.3	Simulation Scenarios	36
5.4	Experiments	40
6	Conclusions and Future Work	45
6.1	Results	45
6.2	Future Work	46
	Bibliography	47
7	Appendix	49

Notation

Symbols and Operators

a_y	Lateral acceleration
β	Slip angle
C_f	Resulting lateral front tire stiffness
C_r	Resulting lateral rear tire stiffness
c_0	Road curvature
c_1	Change of curvature
δ_s	Steering wheel angle
δ	Wheel turn angle
Δ_{v_x}	Velocity measurement resolution
Δ_{δ_s}	Steering wheel angle resolution
\mathbb{E}	Expected mean
e_t	Measurement noise
F_t	Linearized state update matrix
$f_t(\cdot)$	Equations for the system model
G_t	Noise gain matrix
H_t	Linearized measurement relation matrix
h_t	Equations for the measurement model
\mathcal{I}	Identity matrix
J_z	Moment of inertia around z-axis
K_t	Kalman gain
l_f	Distance from masscenter to front wheel
l_r	Distance from masscenter to rear wheel
θ	Heading angle
v_y	Vehicle lateral velocity
v_x	Vehicle longitudinal velocity
W	Lane width
W_{veh}	Vehicle width
y_{off}	Measured lateral offset at vehicle
$y_{off,lc}$	Estimated lateral offset at center of gravity
$y_{off,re}$	Estimated lateral offset to right road edge
P	Covariance matrix
Π_0	Initial uncertainty
$p(\cdot)$	Probability density function

$p(x_t Y_t)$	Posterior density
p_{e_t}	Measurement noise probability function
p_{w_t}	Process noise probability function
Q	Process noise covariance matrix
R	Measurement noise covariance matrix
\mathbb{R}^n	Euclidean n -dimensional space
σ	Standard deviation
T	Sample period
u	Input signal
w_t	Process noise
x_t	State vector at time t
$\hat{x}_{t t}$	Estimate (filtering) at time t
$\hat{x}_{t t-1}$	Estimate (one step prediction) at time t
$\dot{\Psi}$	Yaw rate
\mathbb{Y}_t	The set of ordered measurements: $\mathbb{Y}_t = \{y_1, \dots, y_t\}$
y_t	Measurement at time t
∇	Jacobian operator
\propto	Proportional to
$\lfloor \cdot \rfloor$	Round downwards to nearest integer

Abbreviations

CUSUM	Cumulative Sum
DCC	Distance to Center of Curvature
EKF	Extended Kalman Filter
ESP	Electronic Stability Program
IMU	Inertial Measurement Unit
KF	Kalman Filter
LDWS	Lane Departure Warning System
RMSE	Root Mean Square Error
SF	Sensor Fusion
TtLC	Time to Lane Crossing
VC	Vehicle Coordinates
VD	Vehicle Dynamics

Chapter 1

Introduction

Today passive safety systems such as airbags and seat belts are more or less standard in new cars. A passive safety system does nothing to prevent an accident but merely reduces the consequences of it. An active safety system on the other hand seeks to prevent the actual accident by aiding the driver in case of a dangerous situation. An example of an active safety system is ESP (Electronic Stability Program). One of the most common accident types is when the vehicle simply runs off the road. These kind of accidents could have been prevented if the driver had received a warning just as the vehicle was about to depart from the road or into the opposite lane. The last few years several systems that provide this kind of functionality have reached the market and are called *lane departure warning system* (LDWS). This first generation of LDWS are often based on some sort of monocular camera placed in the windshield. Such a system has both advantages and drawbacks. One big advantage is that the system is based on just one sensor and can be rather cheap; the main drawback is that the system will be sensitive to bad weather and poor road markings. This means that if the driver has problems to see the road, so does the camera. This Master's thesis proposes a system that reduces the drawbacks of a single camera LDWS by using inertial sensors and sensor fusion. The main outlines of the proposed system is described in Figure 1.1.

1.1 Background

1.1.1 Accident Types

A LDWS is supposed to alert the driver if it detects that one of the following accidents [5] are about to happen:

Fast or Slow Unintentional Lane Departure: One of the most common accidents is the unintentional lane departure. This situation is illustrated in Figure 1.2(a). The cause of this accident is that the driver has applied a too large steering angle making the vehicle run off the road. Since the vehicle has

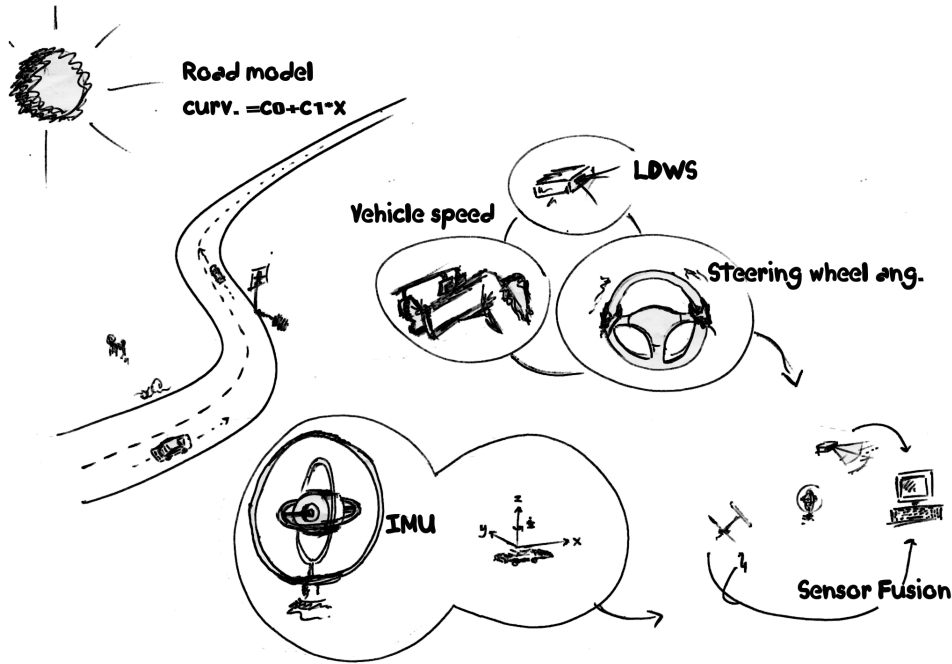


Figure 1.1. A sketch describing the system proposed in this Master's thesis. In following list the different components are described: IMU - measures accelerations and rotational speed, LDWS - measures the lateral position of the vehicle on the road and the road curvature, Road model - the road is modeled online using the measurements from the LDWS, Vehicle speed - lateral speed of the vehicle, Steering wheel angle - the steering wheel angle is measured, Sensor fusion - all measurements are used to estimate interesting vehicle states such as the heading angle.

rather different behavior depending on how rapidly it departs from the road, two subcategories are introduced: Fast Unintentional Lane Departure and Slow Unintentional Lane Departure.

Fast Curve Entering: A fast curve entering is the situation when a vehicle enters a curve with such a high velocity that it risks running off the road. The difference between this category and the former is that in this case the driver has applied a too small steering angle. To detect this kind of situation reliable readings from the camera as well as a good model of the road are needed. The situation is illustrated in Figure 1.2(b).

1.1.2 Sensor Fusion

For a safety system to detect any of the possible dangerous situations described in Figure 1.2, several different sensors are used in this Master's thesis. The separate sensors often provide useful but limited information about what is happening,

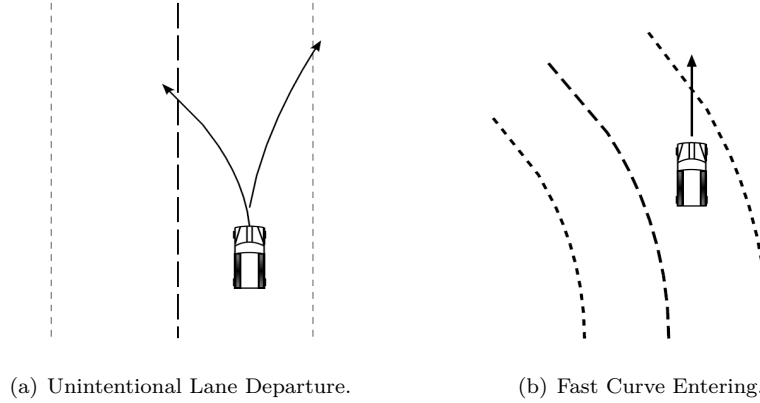


Figure 1.2. Two common accident types. The situation in 1.2(a) is caused by a too large steering angle and the situation in 1.2(b) by a too small steering angle.

hence there is a need to fuse this information to get a more complete and correct estimation of the vehicle states. This can be done using sensor fusion, a method, or rather a collection of many different methods, for combining interesting information from several different data sources, sensors. The sensor fusion method used in this Master's thesis is often known as Bayesian estimation.

1.1.3 Autoliv Electronics

The project that this Master's thesis has been a part of has been conducted at Autoliv Electronics AB. Autoliv Electronics develops safety enhancing products for the automotive industry. For more information about the company, visit www.autoliv.com.

1.2 Problem Definition

Can the performance of a camera based lane departure warning system be enhanced if inertial sensors are added and sensor fusion is used?

1.3 Objectives

The general objective of this Master's thesis is to develop a system which fuses the information gained from a camera based LDWS with inertial measurements from an *inertial measurement unit* (IMU), or in other words, finding a robust solution to the positioning problem using multiple sensors. An evaluation on how the system performs when the confidence in the camera measurements are low, i.e., when a camera based system operates poorly is of course of great interest. Examples of such situations are:

- Fast unintentional lane departure.
- High speed slow unintentional lane departure.
- High speed fast curve entering.

All these situations have in common that there is either a fast lateral or longitudinal motion under which the camera fails to provide reliable readings.

1.4 Limitations

The LDWS that has been used in this Master's thesis is a commercial system producing measurements for a ruled based decision logic. This means that the measurements obtained are heavily manipulated, from what originally must have been rather noisy and unstable measurements. For the derived models this means that it has to deal with measurements having a rather unknown character.

1.5 Outline

In this section a short guidance to the different chapters is given. In Chapter 2 first a description of the sensor fusion technique that have been studied is presented. Chapter 3 describes the models that have been used, starting with a short section on the coordinate systems in which the different models are operating. In the following sections the derivations of the different models are presented. In Chapter 4 a strategy for how to evaluate what the model estimates is presented. Chapter 5 is about how the models have been evaluated. Finally some conclusions and suggestions of future work is given in Chapter 6.

Chapter 2

Sensor Fusion Techniques

The area of *sensor fusion* (SF) is vast and there exists many different terminologies. The topic of different terminologies will not be covered here, but to avoid confusion, in this Master's thesis, the concepts sensor fusion and estimation theory are regarded as synonyms. This chapter covers a short introduction to the benefits of sensor fusion followed by an introduction to Bayesian estimation, the sensor fusion method used in this Master's thesis.

2.1 Advantages of Sensor Fusion

Sensor fusion is motivated if the benefits that can be gained exceeds the cost of the extra sensors. Since all sensors normally are afflicted with inaccuracy, it is not difficult to motivate a good extra sensor and sometimes even an additional sensor that might perform worse than the original one. In the paragraphs below some of the most common problems that can be reduced by SF is presented [6].

Robustness and Redundancy: A multi sensor system has the advantage of being redundant, meaning that if one sensor brakes down or begins to function poorly the system can still work. With robustness it is meant that the system is non-sensitive to noise. For example a camera based LDWS is rather dependent on the weather conditions, whereas a fused system having access to more information can still function properly. These characteristics are of course very attractive for a safety system such as an LDWS.

Measurement Range: Every sensor has limitations in terms of range so there is often a good idea to combine several sensors in order to obtain a fused system with greater working area.

Accuracy: All measurements are affected with some uncertainty which in two dimensions can be represented by a confidence area i.e., the space in which it is believed that the true value is to be found. One common combination when

tracking objects is vision and radar. A vision sensor is typically good at sensing the bearing but poor for distance measures, whereas the radar has the opposite character. The idea is illustrated in Figure 2.1. The two ellipsoids represent two different measurements having different uncertainties. The fused confidence area is then much smaller, namely the area that is cut out by the two ellipsoids.

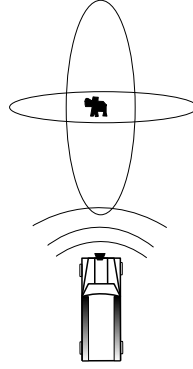


Figure 2.1. Sensor fusion using two different sensors to localize an object.

2.2 Bayesian Estimation

Bayesian estimation [1, 7, 8, 10, 11] offers a way to estimate states from noisy measurements. The following discrete state space description

$$x_{t+1} = f(x_t, w_t), \quad (2.1a)$$

$$y_t = h(x_t, e_t), \quad (2.1b)$$

where the vector $x_t \in \mathbb{R}^n$ represents the sought states and $y_t \in \mathbb{R}^m$ the measurements, is a general model of a dynamic system. Inaccuracies in the process and measurement model are described by the stochastic processes w_t and e_t .

Using the model above and all measurements up until and including time t , $\mathbb{Y}_t \in \{y_1 \dots y_t\}$, an estimate, $\hat{x}_{t|t} \in \mathbb{R}^n$, can be calculated from following equations:

time update:

$$p(x_{t+1}|\mathbb{Y}_t) = \int_{\mathbb{R}^n} p(x_{t+1}|x_t)p(x_t|\mathbb{Y}_t)dx_t, \quad (2.2)$$

measurement update:

$$p(x_t|\mathbb{Y}_t) = \frac{p(y_t|x_t)p(x_t|\mathbb{Y}_{t-1})}{p(y_t|\mathbb{Y}_{t-1})}, \quad (2.3)$$

where p is the *probability density function* (pdf) of two stochastic variables.

In this Master's thesis it will for ease be assumed that the inaccuracies are additive

$$x_{t+1} = f(x_t) + w_t, \quad (2.4a)$$

$$y_t = h(x_t) + e_t. \quad (2.4b)$$

Using the model with additive noise following relations can be calculated

$$p(x_{t+1}|x_t) = p_{w_t}(x_{t+1} - f(x_t)), \quad (2.5a)$$

$$p(y_t|x_t) = p_{e_t}(y_t - h(x_t)). \quad (2.5b)$$

where p_{w_t} is the process noise probability function and p_{e_t} the measurement noise probability function. Using (2.5), the time update (2.2) and the measurement update (2.3) is rewritten as

$$p(x_{t+1}|\mathbb{Y}_t) = \int_{\mathbb{R}^n} p_{w_t}(x_{t+1} - f(x_t))p(x_t|\mathbb{Y}_t)dx_t, \quad (2.6)$$

$$p(x_t|\mathbb{Y}_t) = \frac{p_{e_t}(y_t - h(x_t))p(x_t|\mathbb{Y}_{t-1})}{p(y_t|\mathbb{Y}_{t-1})}, \quad (2.7)$$

and since $p(y_t|\mathbb{Y}_{t-1})$ can be interpreted a normalization factor, (2.7) is written as

$$p(x_t|\mathbb{Y}_t) \propto p_{e_t}(y_t - h(x_t))p(x_t|\mathbb{Y}_{t-1}), \quad (2.8)$$

where \propto should be read proportional to. To solve the Bayesian problem i.e., (2.6) and (2.7) the process model, f and the measurement relation, h , as well as the inaccuracies w_t and e_t must be modeled. If the system is linear and the noise Gaussian the *Kalman filter* (KF) offers a recursive solution to the problem. When the system cannot be assumed linear, a solution is to first linearize the system and then apply a Kalman filter. It is then called an *extended Kalman filter* (EKF).

2.2.1 The Kalman Filter

If a system can be modeled using a linear state space model a Kalman filter [1, 7, 8, 10, 11] can be used. The KF solves the problem of choosing how much of the new information in a measurement that should be included when updating a state-variable. Consider following standard state space model:

$$x_{t+1} = F_t x_t + G_{u,t} u_t + G_{w,t} w_t, \quad (2.9a)$$

$$y_t = H_t x_t + D_t u_t + e_t, \quad (2.9b)$$

where $F_t, G_{u,t}, G_{w,t}, H_t$ and D_t in the general case are time-varying matrices of suitable dimensions, x_t is the state vector, y_t the measurement vector and u_t represents the input signals. The covariances of the state noise, w_t , and the measurement noise, e_t are represented by the Q and R matrices as

$$\text{Cov}(w_t) = Q_t, \quad (2.10a)$$

$$\text{Cov}(e_t) = R_t, \quad (2.10b)$$

if $\mathbb{E}(w_t) = \mathbb{E}(e_t) = 0$ and it is assumed that $\hat{x}_{0|-1} = x_0$, $P_{0|-1} = \Pi_0$ and that the cross covariance is zero the KF equations are given by (2.11a),(2.11b) are

Algorithm 1 Kalman filter (KF)

Time update:

$$\hat{x}_{t+1|t} = F_t \hat{x}_{t|t} + G_{u,t} u_t, \quad (2.11a)$$

$$P_{t+1|t} = F_t P_{t|t} F_t^T + G_{w,t} Q_t G_{w,t}^T, \quad (2.11b)$$

Measurement update:

$$\hat{x}_{t|t} = \hat{x}_{t|t-1} + K_t (y_t - H_t \hat{x}_{t|t-1} - D_t u_t), \quad (2.12a)$$

$$P_{t|t} = P_{t|t-1} - K_t H_t P_{t|t-1}, \quad (2.12b)$$

where

$$K_t = P_{t|t-1} H_t^T (H_t P_{t|t-1} H_t^T + R_t)^{-1}. \quad (2.13)$$

commonly referred to as the time update and (2.12a),(2.12b) as the measurement update equations.

2.2.2 The Extended Kalman Filter

When a linear system is not sufficient, the KF has to be modified. One common choice is the extended Kalman filter [1, 7, 8, 10, 11]. The main idea of the EKF is to linearize around the current state estimate and then use the KF theory. Consider nonlinear time-varying system

$$x_{t+1} = f_t(x_t) + g_t(x_t)w_t, \quad (2.14a)$$

$$y_t = h_t(x_t) + e_t, \quad (2.14b)$$

where w_t and e_t are assumed Gaussian with zero mean and covariances Q_t and R_t , and initial uncertainty Π_0 . Use the following approximations

$$f_t(x_t) \approx f_t(\hat{x}_{t|t}) + F_t(x_t - \hat{x}_{t|t}), \quad (2.15a)$$

$$h_t(x_t) \approx h_t(\hat{x}_{t|t-1}) + H_t(x_t - \hat{x}_{t|t-1}), \quad (2.15b)$$

$$g_t(x_t) \approx g(\hat{x}_{t|t}) = G_t, \quad (2.15c)$$

where

$$F_t^T = \nabla_x f_t^T(x)|_{x=\hat{x}_{t|t}}, \quad H_t^T = \nabla_x h_t^T(x)|_{x=\hat{x}_{t|t-1}}, \quad (2.16)$$

and $\nabla_x f_t^T(x)$ is the Jacobian matrix defined as:

$$\nabla_x f_t^T(x) = \begin{pmatrix} \frac{\partial f_1}{\partial x_1} & \cdots & \frac{\partial f_m}{\partial x_1} \\ \vdots & & \vdots \\ \frac{\partial f_1}{\partial x_n} & \cdots & \frac{\partial f_m}{\partial x_n} \end{pmatrix}, \quad f : \mathbb{R}^n \mapsto \mathbb{R}^m. \quad (2.17)$$

If now (2.14a) and (2.14b) are approximated as

$$x_{t+1} = F_t x_t + \underbrace{(f_t(\hat{x}_{t|t}) - F_t \hat{x}_{t|t})}_{\text{known at time } t} + G_t u_t, \quad (2.18a)$$

$$y_t - \underbrace{(h_t(\hat{x}_{t|t-1}) - H_t \hat{x}_{t|t-1})}_{\text{known at time } t-1} = H_t x_t + e_t, \quad (2.18b)$$

a linear state-space model for x_t is obtained. The KF equations can now be applied resulting in

$$\hat{x}_{t+1|t} = F_t \hat{x}_{t|t} + (f_t(\hat{x}_{t|t}) - F_t \hat{x}_{t|t}) = f(\hat{x}_{t|t}), \quad (2.19a)$$

$$\begin{aligned} \hat{x}_{t|t} &= \hat{x}_{t|t-1} + K_t (y_t - (h_t \hat{x}_{t|t-1} - H_t \hat{x}_{t|t-1}) - H_t \hat{x}_{t|t-1}) \\ &= \hat{x}_{t|t-1} + K_t (y_t - h_t \hat{x}_{t|t-1}), \end{aligned} \quad (2.19b)$$

where the Kalman gain and the covariance recursion is given by the Kalman filter.

Algorithm 2 Extended Kalman filter (EKF)

Time update:

$$\hat{x}_{t+1|t} = f_t(\hat{x}_{t|t}), \quad (2.20a)$$

$$P_{t+1|t} = F_t P_{t|t} F_t^T + G_t Q_t G_t^T, \quad (2.20b)$$

Measurement update:

$$\hat{x}_{t|t} = \hat{x}_{t|t-1} + K_t (y_t - h(\hat{x}_{t|t-1})), \quad (2.21a)$$

$$P_{t|t} = P_{t|t-1} - K_t H_t P_{t|t-1}, \quad (2.21b)$$

where

$$K_t = P_{t|t-1} H_t^T (H_t P_{t|t-1} H_t^T + R_t)^{-1}, \quad (2.22a)$$

$$F_t^T = \nabla_x f_t^T(x)|_{x=\hat{x}_{t|t}}, \quad H_t^T = \nabla_x h^T(x)|_{x=\hat{x}_{t|t-1}}. \quad (2.22b)$$

2.2.3 Sampling of a Continues Time System

Since reality is considered to be continuous, the modeling in this Master's thesis is done in continuous time. Consider the time continuous process model

$$\dot{x}(t) = Ax(t) + B_u u(t) + B_w w(t), \quad (2.23)$$

where A , B_u and B_w are variable matrices of suitable dimensions. The filtering however is done in discrete time, thus a sampling formula for (2.9) is needed. A very simple approach is to perform a backwards difference [9]

$$\dot{x}(t) \approx \frac{1}{T} (x(t+T) - x(t)), \quad (2.24)$$

where T is the period of the sampling rate. A more accurate method to obtain a discrete model is to integrate the model over a period $[t_0, t_0 + T]$ under which the signal $u(t)$ is constant

$$x_{t+T} = x_t + \int_t^{t+T} (Ax_\tau + B_u u_\tau) d\tau. \quad (2.25)$$

The solution to (2.25) then forms the discrete state space representation:

$$x_{t+T} = F_t x_t + G_u u_t, \quad (2.26a)$$

$$F_t = e^{(AT)}, \quad (2.26b)$$

$$G_u = \int_0^T e^{(AT)} B_u d\tau. \quad (2.26c)$$

If (2.25) cannot be solved analytically a numerical approximation is needed. One possibility is to expand $F_t = e^{(AT)}$ in a Taylor series. If the Taylor expansion is truncated so that only the linear part remains, same result as if using (2.24) is obtained.

Chapter 3

Vehicle and Sensor Models

In Chapter 2 it became clear that in order to solve the Bayesian problem it must be modeled how the system propagates in time and how the measurements are related to the sought states as well as how accurate these models are. With the notation in this Master's thesis the task is to find the deterministic nonlinear functions f and h and the stochastic processes w_t and e_t .

3.1 Coordinate Systems

3.1.1 Vehicle Coordinates

In this section the *vehicle coordinate* (VC) system is defined, which will be the reference system in which the remaining derivation is performed. The vehicle coordinate presented in Figure 3.1, is a Cartesian coordinate system rigidly attached to the vehicle center of gravity, i.e., if the vehicle moves so will the coordinate system. The systems' axes will here be denoted (x_v, y_v) .

3.1.2 Sensor Coordinates

Inertial Measurement Unit: The inertial measurement unit measures in a Cartesian coordinate system rigidly attached to the center of the unit, as is illustrated in Figure 3.2. The measurements used in this Master's thesis are the yaw rate, $\dot{\Psi}$ and the lateral acceleration a_y . The definition of the yaw rate as can be seen in Figure 3.2 is the counterclockwise rotational speed around the z-axis.

Lane Departure Warning System Coordinates: The lane departure warning system measures properties of the road, such as curvature and width. It also measures the vehicle lateral position relative to the road so there is no need to define an extra coordinate system for the LDWS since this is already compensated for internally.

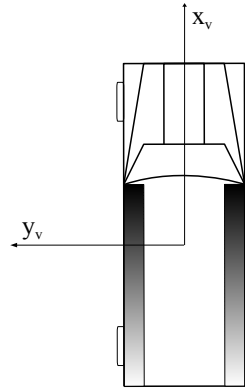


Figure 3.1. Vehicle coordinate system where the x-axis is directed in the vehicle's longitudinal direction and the y-axis in the lateral direction, such that the z-axis points upwards in a right ON-basis.

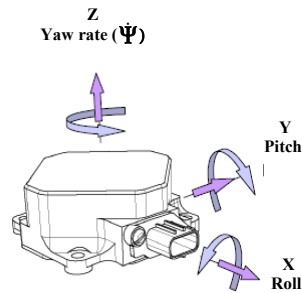


Figure 3.2. The IMU coordinate system is aligned with the VC system, i.e., the x-axis points in the longitudinal direction.

3.2 Process Model

The process model aims at describing the lateral movement of the vehicle. There are many different models of varying complexity suggested in the literature. Here a model with two degrees of freedom is used. The derivation is similar to the ones found in [12] and [13].

3.2.1 Movement in Vehicle Coordinates

The measurements from the IMU are given in vehicle coordinates. In Figure 3.3 the future position (time t) is expressed in the vehicle coordinate system at the current position (time 0) relative some system rigidly attached to the ground, here denoted (x_{fix}, y_{fix}) .

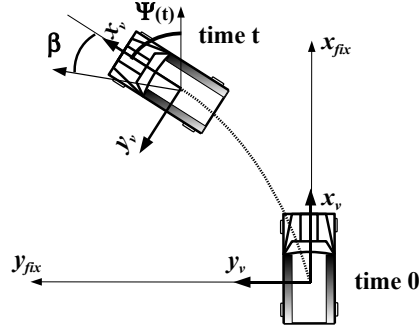


Figure 3.3. The predicted path of the vehicle.

$$V_x^{fix}(t) = v_x^v(t) \cos \Psi(t) - v_y^v(t) \sin \Psi(t), \quad (3.1a)$$

$$V_y^{fix}(t) = v_x^v(t) \sin \Psi(t) + v_y^v(t) \cos \Psi(t). \quad (3.1b)$$

If it is assumed that Ψ and the absolute lateral velocity, v_y^v , is small during the prediction interval, the following relations are obtained:

$$V_x^{fix} = v_x^v, \quad (3.2a)$$

$$V_y^{fix} = v_x^v \Psi(t) + v_y^v. \quad (3.2b)$$

From (3.2a) we see that the time derivative of the longitudinal velocity is zero for a short time period. The longitudinal acceleration can therefore be modeled as

$$\dot{v}_x = w(t), \quad (3.3)$$

where $w(t)$ is Gaussian noise. (3.2b) will be explained in section 3.2.5.

3.2.2 The Bicycle Model

In this section a *vehicle dynamics* (VD) model, commonly known as the bicycle model [12, 13], is derived. The reason for the name bicycle comes from that the model considers the wheels on each axis as a single unit, as in Figure 3.4, where also all variables needed for the derivations in this section is defined. If now the forces

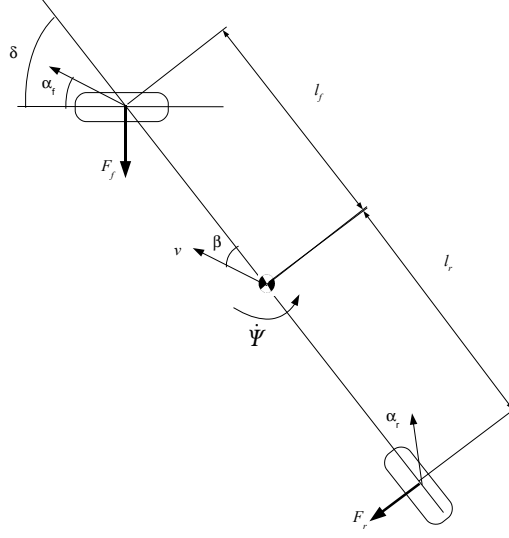


Figure 3.4. The bicycle model considers the the wheels on each axis as single unit. The variables for the bicycle model are: F_f - lateral front wheel force, F_r - lateral rear wheel force, δ - wheel turn angle, α_f - tire side slip angle front, α_r - tire side slip angle rear, β - vehicle body side slip angle, l_f - distance from center of gravity to front axle, l_r - distance from center of gravity to rear axle.

F_r and F_f defined in Figure 3.4 are summed in y_v -direction and Newton's second law is used under the assumption that the centripetal acceleration is directed toward the center of curvature and the angles are small, the following equations are obtained

$$F_f \cos \delta + F_r = ma_n, \quad (3.4a)$$

$$F_f \cos \delta l_f - F_r \cdot l_r = J_z \ddot{\Psi}, \quad (3.4b)$$

where m is the vehicle mass and $\ddot{\Psi}$ is the angular acceleration around the z-axis in the VC system and J_z the moment of inertia around the z-axis. The

centripetal acceleration, a_n , can be written as a sum of the lateral acceleration and the redirection of the longitudinal velocity

$$a_n = \dot{v}_y + v_x \dot{\Psi}. \quad (3.5)$$

To find expressions for the forces F_f and F_r it is assumed that they can be written as linear functions of the tire side slip angles, here denoted α_f and α_r . This is a sufficiently good approximation at least for slip angles less than 4° [13].

$$F_f = 2C_f \cdot \alpha_f, \quad (3.6a)$$

$$F_r = 2C_r \cdot \alpha_r, \quad (3.6b)$$

where C_f and C_r are the cornering stiffnesses for the front respectively the rear [13]. To find the slip angles, the velocities v_f and v_r must first be calculated. In Figure 3.5 the relations between the different angles are illustrated. To find a linear

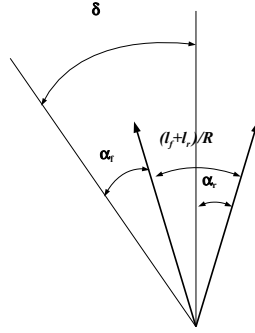


Figure 3.5. Relations between the wheel turn angle, δ and the tire side slip angles α_f and α_r .

relation for the angles, the velocity of the front wheel v_f , is written as $(v_x, v_y + l_f \dot{\Psi})$ and the velocity of the rear wheel $(v_x, -v_y + l_r \dot{\Psi})$. Then from Figure 3.5 following expressions are derived:

$$\tan(\delta - \alpha_f) = \frac{v_y + l_f \dot{\Psi}}{v_x}, \quad (3.7a)$$

$$\tan(\alpha_r) = \frac{-v_y + l_r \dot{\Psi}}{v_x}. \quad (3.7b)$$

If now (3.5), (3.6) and (3.7) are inserted into (3.4), the following system is obtained

$$\begin{pmatrix} \ddot{\Psi} \\ \dot{v}_y \end{pmatrix} = \begin{pmatrix} \frac{1}{J_z} \left(2C_f l_f \cos \delta \left(\delta - \arctan\left(\frac{v_y + l_f \dot{\Psi}}{v_x}\right) \right) - 2C_f l_r \left(\arctan\left(\frac{-v_y + l_r \dot{\Psi}}{v_x}\right) \right) \right) + \delta \frac{2l_f C_f}{J_z} \\ \frac{1}{m} \left(2C_f \cos \delta \left(\delta - \arctan\left(\frac{v_y + l_f \dot{\Psi}}{v_x}\right) \right) + 2C_r \left(\arctan\left(\frac{-v_y + l_r \dot{\Psi}}{v_x}\right) \right) \right) + \delta \frac{2C_f}{m} \end{pmatrix}. \quad (3.8)$$

To obtain simpler expressions it is assumed that the wheel turn angle and the side slip angles can be considered small. Under these assumptions (3.7) simplifies to

$$\alpha_f = \delta - \frac{v_y + l_f \dot{\Psi}}{v_x}, \quad (3.9a)$$

$$\alpha_r = \frac{-v_y + l_r \dot{\Psi}}{v_x}. \quad (3.9b)$$

Inserting (3.5) and (3.9) into (3.4) the following is obtained:

$$C_f \left(\delta - \frac{v_y + l_f \dot{\Psi}}{v_x} \right) + C_r \left(\frac{-v_y + l_r \dot{\Psi}}{v_x} \right) = m(\dot{v}_y + v_x \dot{\Psi}), \quad (3.10a)$$

$$C_f \left(\delta - \frac{v_y + l_f \dot{\Psi}}{v_x} \right) l_f - C_r \left(\frac{-v_y + l_r \dot{\Psi}}{v_x} \right) l_r = J_z \ddot{\Psi}, \quad (3.10b)$$

which after some reformulation is written as:

$$\begin{pmatrix} \ddot{\Psi} \\ \dot{v}_y \\ \dot{v}_x \\ \dot{\delta} \end{pmatrix} = \begin{pmatrix} f_{11} \dot{\Psi}/v_x + f_{12} v_y/v_x + f_{13} \delta \\ (-v_x + f_{21}/v_x) \dot{\Psi} + f_{22} v_y/v_x + f_{23} \delta \\ 0 \\ 0 \end{pmatrix} + w(t) \quad (3.11)$$

where

$$f_{11} = \frac{2}{J_z} (-l_f^2 C_f - l_r^2 C_r), \quad (3.12a)$$

$$f_{12} = \frac{2}{J_z} (-l_f C_f + l_r C_r), \quad (3.12b)$$

$$f_{13} = \frac{2l_f C_f}{J_z}, \quad (3.12c)$$

$$f_{21} = \frac{-2C_f l_f + 2C_r l_r}{m}, \quad (3.12d)$$

$$f_{22} = \frac{-2C_f - 2C_r}{m}, \quad (3.12e)$$

$$f_{23} = \frac{2C_f}{m}, \quad (3.12f)$$

and w_t is Gaussian noise. This model is nonlinear and therefore KF cannot be used. However it is possible to obtain a structure that allows KF if the longitudinal velocity, v_x , and the wheel turn angle, δ , are considered input signals. The equations are still the same but can now be written on state space form as:

$$\begin{pmatrix} \ddot{\Psi} \\ \dot{v}_y \end{pmatrix} = \begin{pmatrix} a_{11}(v_x) & a_{12}(v_x) \\ a_{21}(v_x) & a_{22}(v_x) \end{pmatrix} \begin{pmatrix} \dot{\Psi} \\ v_y \end{pmatrix} + \begin{pmatrix} b_1 \\ b_2 \end{pmatrix} \delta + w(t), \quad (3.13)$$

where

$$a_{11} = \frac{2}{v_x J_z} (-l_f^2 C_f - l_r^2 C_r), \quad (3.14a)$$

$$a_{12} = \frac{2}{v_x J_z} (-l_f C_f + l_r C_r), \quad (3.14b)$$

$$a_{21} = -v_x - \frac{-2C_f l_f + 2C_r l_r}{m v_x}, \quad (3.14c)$$

$$a_{22} = \frac{-2C_f - 2C_r}{m v_x}, \quad (3.14d)$$

$$b_1 = \frac{2l_f C_f}{J_z}, \quad (3.14e)$$

$$b_2 = \frac{2C_f}{m}, \quad (3.14f)$$

$w(t)$ is Gaussian noise and δ is the wheel turn angle.

3.2.3 Road Model

In this section a model for describing the lane-edge geometry in vehicle coordinates is derived, similarly to the one found in [4]. A road is constructed by segments which are either straight or curved and the transition between these segments is done with clothids. A clothid is a curve where the curvature changes linearly with the length of the clothid. To describe a clothid we will first define the curvature as the inverse radius of curvature,

$$c(l) = \frac{1}{R(l)}. \quad (3.15)$$

Next the clothid parameter Λ is defined as:

$$\Lambda^2 = R(L) \cdot L = \frac{1}{c_1}, \quad (3.16)$$

where c_1 is the change of curvature at the end point, $l = L$. The curvature can now be expressed as:

$$c(l) = c_0 + c_1 \cdot l \quad (3.17)$$

where c_0 is the curvature at the starting point $l = 0$.

Next the curvature function (3.17) is derived with respect to time,

$$\frac{dc}{dt} = \frac{dc}{dl} \cdot \frac{dl}{dt} = c_1 \cdot v. \quad (3.18)$$

From (3.15) we also see that the time derivative of c_1 can be written as:

$$\frac{dc_1}{dt} = \frac{d}{dt} \cdot \frac{1}{\Lambda^2} = 0. \quad (3.19)$$

Finally this is written on state space form as:

$$\begin{aligned} \dot{c}_0 &= c_1 \cdot v, \\ \dot{c}_1 &= 0. \end{aligned} \quad (3.20)$$

3.2.4 Heading Angle

Now that the models for the vehicle and the road have been derived, the next step is to connect them. To do this the fact that the yaw angle, Ψ , and the heading angle, θ , are connected through some fix reference, here denoted γ , is used. This is illustrated in Figure 3.6 and the equation describing the situation is:

$$\theta = \Psi - \gamma. \quad (3.21)$$

To obtain a relation between θ and Ψ the time derivative of θ is taken

$$\dot{\theta} = \dot{\Psi} - \dot{\gamma} \approx \dot{\Psi} - \frac{v}{R} = \dot{\Psi} - c(l)v \approx \dot{\Psi} - c_0 v. \quad (3.22)$$

Here v is the current velocity, R is the road curvature and $\dot{\Psi}$ is the yaw rate. The relations are illustrated in Figure 3.6. Here it has been used that the *displacement in center of curvature* (DCC) is small and therefore the approximation $\dot{\gamma} \approx \frac{v}{R}$ can be used. The second approximation made is $c(l) \approx c_0$, allowed since the distance from the camera to where the curvature is measured is small.

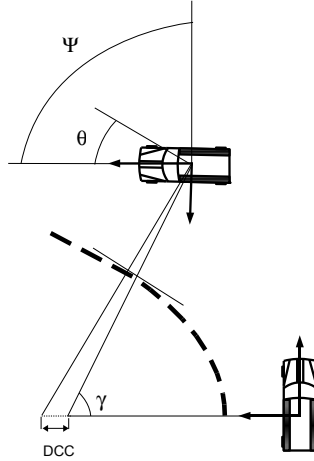


Figure 3.6. The connection between the heading angle (θ) and the yaw angle (Ψ). The displacement in center of curvature is considered small.

3.2.5 Lateral Position on the Road

In this section the equations describing the lateral position on the road is derived, using what has been derived in the previous sections. In Section 3.2.1 the movement in VC is derived this describes how the vehicle is moving relative its old position. Now to find the movement relative to the road, the yaw angle Ψ is

substituted for the heading angle θ . Assuming that the width of the road remains constant under the prediction interval the following relations hold:

$$W/2 = y_{off,c} - y_{off,re}, \quad (3.23a)$$

$$\dot{W}/2 = 0 \Rightarrow \dot{y}_{off,c} = \dot{y}_{off,re}. \quad (3.23b)$$

From (3.1b) following is obtained:

$$\dot{y}_{off,c} = v_x \sin(\theta) + v_y \cos(\theta). \quad (3.24)$$

If small angles is assumed, (3.24) reduces to:

$$\dot{y}_{off,c} = v_x \theta + v_y. \quad (3.25)$$

3.2.6 Process Model - Summary

In this section the complete model is presented.

Nonlinear Model: The continuous nonlinear model is written in the form:

$$\dot{x}(t) = f(x(t)) + w(t) \quad (3.26)$$

where

$$x(t) = \begin{pmatrix} x_1 \\ x_2 \\ x_3 \\ x_4 \\ x_5 \\ x_6 \\ x_7 \\ x_8 \\ x_9 \end{pmatrix} = \begin{pmatrix} \dot{\Psi} \\ v_y \\ c_0 \\ c_1 \\ \theta \\ y_{off,c} \\ y_{off,re} \\ v_x \\ \delta \end{pmatrix}, \quad (3.27a)$$

$$f(x(t)) = \begin{pmatrix} \frac{1}{J_z} \left(2C_f a \cos \delta \left(\delta - \arctan\left(\frac{v_y + l_f \dot{\Psi}}{v_x}\right) \right) - 2C_f l_r \left(\arctan\left(\frac{-v_y + l_r \dot{\Psi}}{v_x}\right) \right) \right) + \delta \frac{2l_f C_f}{J_z} \\ \frac{1}{m} \left(2C_f \cos \delta \left(\delta - \arctan\left(\frac{v_y + l_f \dot{\Psi}}{v_x}\right) \right) - 2C_r \left(\arctan\left(\frac{-v_y + l_r \dot{\Psi}}{v_x}\right) \right) \right) + \delta \frac{2C_f}{m} \\ c_1 v_x \\ 0 \\ \dot{\Psi} - (c_0 + c_1 l_f) v_x \\ v_x \sin(\theta) + v_y \cos(\theta) \\ v_x \sin(\theta) + v_y \cos(\theta) \\ 0 \\ 0 \end{pmatrix}. \quad (3.27b)$$

If small angles are assumed (3.27b) reduces to

$$f(x(t)) = \begin{pmatrix} f_{11}\dot{\Psi}/v_x + f_{12}v_y/v_x + b_1\delta \\ (-v_x - f_{21}/v_x)\dot{\Psi} + f_{22}v_y/v_x + b_2\delta \\ c_1v_x \\ 0 \\ \dot{\Psi} - c_0v_x \\ v_x \sin(\theta) + v_y \cos(\theta) \\ v_x \sin(\theta) + v_y \cos(\theta) \\ 0 \\ 0 \end{pmatrix}. \quad (3.28)$$

KF-Model:

$$\dot{x} = A(v(x))x(t) + Bu + w(t), \quad (3.29)$$

$$x(t) = \begin{pmatrix} x_1 \\ x_2 \\ x_3 \\ x_4 \\ x_5 \\ x_6 \\ x_7 \end{pmatrix} = \begin{pmatrix} \dot{\Psi} \\ v_y \\ c_0 \\ c_1 \\ \theta \\ y_{off,c} \\ y_{off,re} \end{pmatrix}, \quad (3.30a)$$

$$A(v(x)) = \begin{pmatrix} a_{11} & a_{12} & 0 & 0 & 0 & 0 & 0 \\ a_{21} & a_{22} & 0 & 0 & 0 & 0 & 0 \\ 0 & 0 & 0 & v_x & 0 & 0 & 0 \\ 0 & 0 & 0 & 0 & 0 & 0 & 0 \\ 1 & 0 & -v_x & 0 & 0 & 0 & 0 \\ 0 & 1 & 0 & 0 & v_x & 0 & 0 \\ 0 & 1 & 0 & 0 & v_x & 0 & 0 \end{pmatrix}, \quad B = \begin{pmatrix} b_1 \\ b_2 \\ 0 \\ 0 \\ 0 \\ 0 \\ 0 \end{pmatrix}. \quad (3.30b)$$

3.2.7 Process Noise - Piecewise Constant Acceleration

The process noise is modeled in discrete time under the assumption that the vehicle undergoes a constant acceleration w_t each sampling period and that these accelerations are uncorrelated from period to period, i.e., a piecewise constant acceleration [2, 3]. If the vehicle undergoes a constant acceleration for a time period

T , the increment in velocity is $v_t T$ and in position $v_t T^2/2$. To illustrate how this is modeled the submatrices for the heading angle are modeled as

$$x^\Psi = (\dot{\Psi} \quad \theta)^T \quad (3.31a)$$

$$G_{w,t}^\Psi = (T \quad T^2/2)^T. \quad (3.31b)$$

This is now applied to the whole system and following two process noise models are obtained:

Extended Kalman Filter - Process Noise Model:

$$G_{w,t} = \begin{pmatrix} T & 0 & 0 & 0 & 0 \\ 0 & T & 0 & 0 & 0 \\ 0 & 0 & \frac{T^2}{2} & 0 & 0 \\ 0 & 0 & \frac{T^2}{2} & 0 & 0 \\ \frac{T^2}{2} & 0 & 0 & 0 & \frac{T^2}{2} \\ \frac{T^2}{2} & \frac{T^2}{2} & 0 & 0 & 0 \\ \frac{T^2}{2} & \frac{T^2}{2} & 0 & 0 & 0 \\ 0 & 0 & 0 & T & 0 \\ 0 & 0 & 0 & 0 & \frac{T^2}{2} \end{pmatrix}, \quad (3.32a)$$

$$Q = Cov(w_t) = \begin{pmatrix} \sigma_\Psi^2 & 0 & 0 & 0 & 0 \\ 0 & \sigma_y^2 & 0 & 0 & 0 \\ 0 & 0 & \sigma_{c_0}^2 & 0 & 0 \\ 0 & 0 & 0 & \sigma_x^2 & 0 \\ 0 & 0 & 0 & 0 & \sigma_\delta^2 \end{pmatrix}. \quad (3.32b)$$

According to [3] σ should be of the order the maximum acceleration magnitude. This is considered a guideline in this Master's thesis.

Kalman Filter - Process Noise Model: The KF model has a smaller Q -matrix since the wheel turn angle and the velocity are regarded input signals.

$$Q = Cov(w_t) \begin{pmatrix} \sigma_\Psi^2 & 0 & 0 \\ 0 & \sigma_y^2 & 0 \\ 0 & 0 & \sigma_{c_0}^2 \end{pmatrix}, \quad (3.33a)$$

$$G_{w,t} = \begin{pmatrix} T & 0 & 0 \\ 0 & T & 0 \\ 0 & 0 & \frac{T^2}{2} \\ 0 & 0 & T \\ \frac{T^2}{2} & 0 & \frac{T^2}{2} \\ 0 & \frac{T^2}{2} & 0 \\ 0 & \frac{T^2}{2} & 0 \end{pmatrix} \quad (3.33b)$$

3.3 Measurement Model

In this section the connections between the measurements and the states are modeled. When a measurement and a state are represented using the same symbol, an upper index m is used to denote measurement.

3.3.1 Road Vehicle Geometry

To be able to build the measurement model properly, all distances and angles connecting the measurements with states describing the vehicle movement on the road must be found. In Figure 3.7 the geometry between the vehicle and road is described. The LDWS measures the distance from the center of the front of the vehicle to the center of the lane.

3.3.2 Yaw Rate and Lateral Acceleration

The yaw rate and the lateral acceleration are both measured by the IMU and hence they have similar characteristics. Inertial measurements are indeed very robust and reliable in the sense that they are not influenced by weather conditions nor by other exterior conditions. However, an IMU rarely provides us with nice data; instead they are afflicted by errors like drift, scaling, offset, etc. In this Master's thesis only offset is considered and the remaining errors are modeled as white noise. This is done since the other errors are more difficult to model and would be hard to observe. The offset is modeled as:

$$\bar{x}_{t+1} = \begin{pmatrix} f_t(x_t) \\ b_t \end{pmatrix} + \begin{pmatrix} g_t(x_t) \\ 0 \end{pmatrix} w_t, \quad (3.34a)$$

$$y_t = h_t(x_t) + b_t + e_t, \quad (3.34b)$$

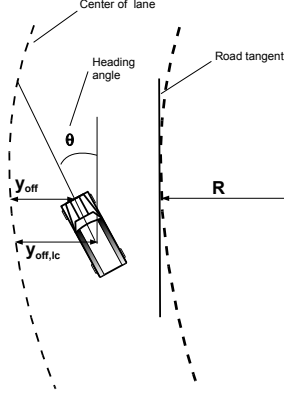


Figure 3.7. Road Vehicle geometry.

which on standard state space form is written

$$\bar{x}_{t+1} = \begin{pmatrix} F_t & 0 \\ 0 & \mathcal{I} \end{pmatrix} \begin{pmatrix} x_t \\ b_t \end{pmatrix} + \begin{pmatrix} G_{w,t} \\ 0 \end{pmatrix} w_t, \quad (3.35a)$$

$$y_t = \begin{pmatrix} H_t & \mathcal{I} \end{pmatrix} \begin{pmatrix} x_t \\ b_t \end{pmatrix} + D_t u_t + e_t, \quad (3.35b)$$

where \mathcal{I} denotes the identity matrix. The yaw rate measurement and the lateral acceleration measurement are now modeled as:

$$\dot{\Psi}_t^m = \dot{\Psi}_t + b_{t,\dot{\Psi}} + e_{t,\dot{\Psi}}, \quad (3.36a)$$

$$a_{t,y}^m = (-v_{t,x} - f_{21}/v_{t,x})\dot{\Psi} + f_{22}v_{t,y}/v_{t,x} + b_{t,a_y} + e_{t,a_y}. \quad (3.36b)$$

where $b_{t,\dot{\Psi}}$ denotes the estimated yaw rate offset and b_{t,a_y} the estimated offset on the lateral acceleration measurement. The reason for that equation (3.36b) cannot be expressed as (3.36a), i.e., directly connected to a state a_y is that the lateral acceleration is already there via equation (3.5) and hence it must be modeled using Newton's second law. In Figure 3.8 the lateral acceleration is measured as the vehicle was standing still, i.e., it should be zero but instead approximately gaussian noise with an offset of 0.35 m/s^2 .

3.3.3 Lateral Offset

In Figure 3.9(a) the geometry needed to derive the equation that connects the lateral offset that the camera measures, to the lateral offset of center of gravity, is presented. The reason for this is that since the IMU measures the movement of the center of gravity so must the states representing the lateral offset. This

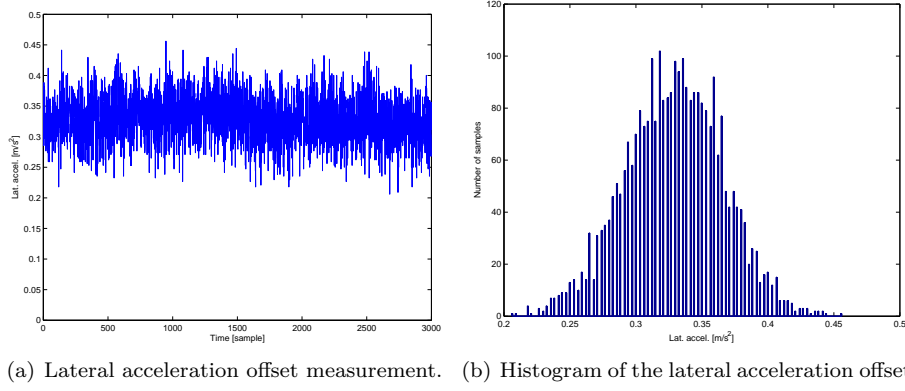


Figure 3.8. Lateral acceleration offset measurement.

derivation is similar to the one found in [14]. First the geometric connections for the sought states are written as:

$$y_{off,c} = |d| + (|f| - |c|), \quad (3.37a)$$

$$y_{off,re} = |e| + (|g| - |d|). \quad (3.37b)$$

The distances d, f and e are found from:

$$d = l_f \sin(\theta) \approx l_f \theta, \quad (3.38a)$$

$$f = y_{off} \cos(\theta) \approx y_{off}, \quad (3.38b)$$

$$e = l_f \sin(\theta) \approx l_f \theta. \quad (3.38c)$$

To find an expression for c a little bit more geometry is needed:

$$\begin{aligned} R^2 &= (R - c)^2 + (l_f \cos(\theta) + y_{off} \sin(\theta))^2 \Rightarrow \\ 2Rc - c^2 &= l_f^2 \cos^2(\theta) + 2ay_{off} \cos(\theta) \sin(\theta) + y_{off}^2 \sin^2(\theta). \end{aligned} \quad (3.39)$$

In (3.38a) the Pythagorean theorem has been used if now it is assumed that c and θ is small following expression is obtained:

$$c = \frac{l_f^2 + 2ay_{off}\theta + y_{off}^2\theta^2}{2R}. \quad (3.40)$$

The last approximation needed to obtain a linear expression uses that the contributions from the terms containing θ is small in comparison to a^2 , thus allowing us to neglect them. The distance c is then finally written as:

$$c = \frac{l_f^2}{2R}. \quad (3.41)$$

Now (3.37) can be written as:

$$y_{off,c} = l_f \theta + y_{off} - \frac{l_f^2}{2R}, \quad (3.42a)$$

$$y_{off,re} = l_f \theta + W/2 + y_{off} - \frac{l_f^2}{2R}, \quad (3.42b)$$

and from (3.42), the desired measurement equations are obtained:

$$y_{off} = \frac{l_f^2}{2R} + y_{off,c} - l_f \theta, \quad (3.43a)$$

$$W/2 + y_{off} = \frac{l_f^2}{2R} + y_{off,re} - l_f \theta. \quad (3.43b)$$

Adaptive Lateral Offset Variance: Since the measurements from the LDWS is highly dependent on weather conditions, if there are any road markings etc., there is a need to include this change of variance in the model. From LDWS a confidence estimate $R_{y_{off}}$ in percent is given. 0% means that system has no confidence in the offset measurement and 100% means that the system regards the measurement as perfect.

$$\sigma_{y_{off}} = \frac{2.5}{1 + R_{y_{off}}}, \quad (3.44a)$$

$$\sigma_{y_{off}} \in [0.0248, 2.5][m], \quad (3.44b)$$

where the constants in (3.44a) are chosen so that $\sigma_{y_{off}}$ has the almost the same range as y_{off} .

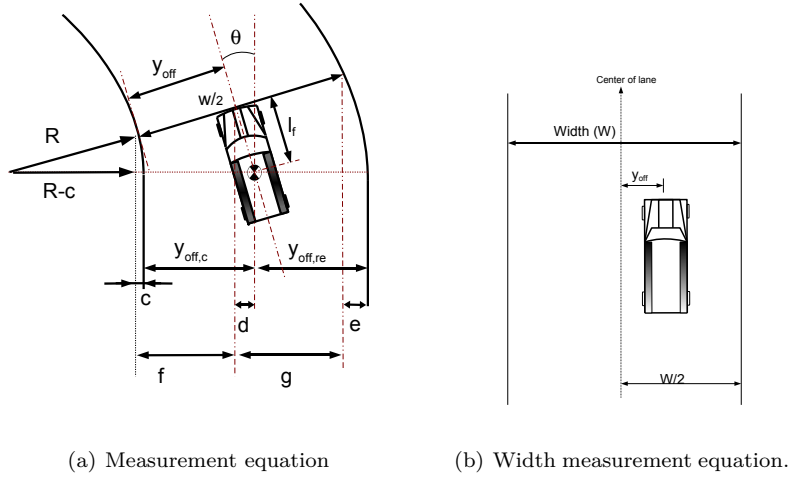


Figure 3.9. The geometry used in the measurement equation.

3.3.4 Lane Width

Figure 3.9(b) illustrates how the width of the lane is measured and how this is connected to the lateral offset measurement. For completeness, the measurement equations that use the width is given as

$$W/2 + y_{off} = \frac{l_f^2}{2R} + y_{off,re} - l_f\theta. \quad (3.45)$$

3.3.5 Road Curvature

The curvature is here defined as being positive when the road turns to the right. Since there is no possibility to observe an offset, drift etc., for this measurement all noise will be modeled as white:

$$c_0^m = c_0 + v_{c_0}, \quad (3.46a)$$

$$v_{c_0} \in N(0, \sigma_{c_0}). \quad (3.46b)$$

Adaptive Curvature Variance: The curvature variance similarly to the the lateral offset variance,

$$\sigma_{c_0} = \frac{0.008}{1 + R_{y_{off}}}, \quad (3.47)$$

resulting in the adaptive standard deviation:

$$\sigma_{c_0} \in [7.93 \cdot 10^{-5}, 0.008][1/m]. \quad (3.48)$$

3.3.6 Vehicle Speed and Wheel Turn Angle

Both the vehicle speed and the wheel turn angle measurements are simply taken as true and low pass filtered. Since it is the steering wheel angle that is measured and not the wheel turn angle this measurement is scaled a factor 20 [12].

$$v_x^m = v_x + e_t, \quad (3.49)$$

$$\delta_m = \delta_s/20 + e_t, \quad (3.50)$$

where $\delta_s/20 = \delta$.

3.3.7 Measurement Model - Summary

In this section the complete measurement models are presented.

EKF Measurement Model:

$$\bar{x}_t = \begin{pmatrix} x_1 \\ x_2 \\ x_3 \\ x_4 \\ x_5 \\ x_6 \\ x_7 \\ x_8 \\ x_9 \\ x_{10} \\ x_{11} \end{pmatrix} = \begin{pmatrix} \dot{\Psi} \\ v_y \\ c_0 \\ c_1 \\ \theta \\ y_{off,c} \\ y_{off,re} \\ v_x \\ \delta \\ b_{\Psi} \\ b_{a_y} \end{pmatrix}, \quad (3.51a)$$

$$y_t = \begin{pmatrix} y_1 \\ y_2 \\ y_3 \\ y_4 \\ y_5 \\ y_6 \\ y_7 \end{pmatrix} = \begin{pmatrix} \dot{\Psi}^m \\ c_0^m \\ y_{off} \\ W/2 + y_{off} \\ v_x^m \\ \delta^m \\ a_y \end{pmatrix}, \quad (3.51b)$$

$$h_t(x_t) = \begin{pmatrix} \dot{\Psi} + b_{\Psi} \\ c_0 \\ l_f^2 c_0 / 2 + y_{off,cl} - l_f \theta \\ l_f^2 c_0 / 2 + y_{off,re} - l_f \theta \\ v_x \\ \delta \\ (-v_x - f_{21}/v_x) \dot{\Psi} + f_{22} v_y / v_x + b_2 \delta + b_{a_y} \end{pmatrix}. \quad (3.51c)$$

KF Measurement Model:

$$\bar{x}_t = \begin{pmatrix} x_1 \\ x_2 \\ x_3 \\ x_4 \\ x_5 \\ x_6 \\ x_7 \\ x_8 \\ x_9 \end{pmatrix} = \begin{pmatrix} \dot{\Psi} \\ v_y \\ c_0 \\ c_1 \\ \theta \\ y_{off,c} \\ y_{off,re} \\ b_{\Psi} \\ b_{a_y} \end{pmatrix}, \quad (3.52a)$$

$$y_t = \begin{pmatrix} y_1 \\ y_2 \\ y_3 \\ y_4 \\ y_5 \end{pmatrix} = \begin{pmatrix} \dot{\Psi}^m \\ c_0^m \\ y_{off} \\ W/2 + y_{off} \\ a_y \end{pmatrix}, \quad (3.52b)$$

$$H_t = \begin{pmatrix} 1 & 0 & 0 & 0 & 0 & 0 & 0 & 1 & 0 \\ 0 & 0 & 1 & 0 & 0 & 0 & 0 & 0 & 0 \\ 0 & 0 & l_f^2/2 & 0 & -l_f & 1 & 0 & 0 & 0 \\ 0 & 0 & l_f^2/2 & 0 & -l_f & 0 & 1 & 0 & 0 \\ a_{21}(v_x) & a_{22}(v_x) & 0 & 0 & 0 & 0 & 0 & 0 & 1 \end{pmatrix}, \quad (3.52c)$$

$$D_t = \begin{pmatrix} 0 \\ 0 \\ 0 \\ 0 \\ b_2 \end{pmatrix}, \quad u_t = \delta_t. \quad (3.52d)$$

Chapter 4

Decision Strategies

To give accurate warnings not only a good model and well interpreted measurements are needed, but also a good decision strategy is necessary. A decision strategy is the way that the information in the states is used to make a decision to alert the driver. In this Master's thesis two complementary techniques are presented, time to lane crossing and CUSUM-test.

4.1 Time to Lane Crossing

Time to lane crossing (TtLC) is the manoeuvre time that the driver has before the vehicle departs from the lane. Two models for calculating the TtLC are suggested in [16], here the simpler one is used. The TtLC approximation is calculated as:

$$TtLC = \frac{W/2 - W_{veh}/2 - y_{off,c}}{\dot{y}_{off,c}} \approx \frac{W/2 - W_{veh}/2 - y_{off,c}}{v_y + \theta v_x}, \quad (4.1)$$

where W_{veh} is the width of the vehicle.

4.2 CUSUM-test for Detecting Lane Departure

In this section it is described how a simple *cumulative sum* (CUSUM)-test [8, 15] can be used to detect a lane departure when the TtLC fails. The idea is illustrated in Figure 4.1. As long as a KF is working properly, the innovations from the filter should be Gaussian noise. However, if a sudden change occurs this does not apply, instead the mean might have increased, indicating that something has happened. The innovations, denoted e_t and its covariance matrix, denoted S_t , are defined as:

$$e_t = y_t - H_t \hat{x}_{t|t-1}, \quad (4.2a)$$

$$S_t = H_t P_{t|t-1} H_t^T + R_t. \quad (4.2b)$$

A normalized distance measure s_t [8] can now be defined as:

$$s_t = S_t^{-1/2} e_t, \quad (4.3)$$

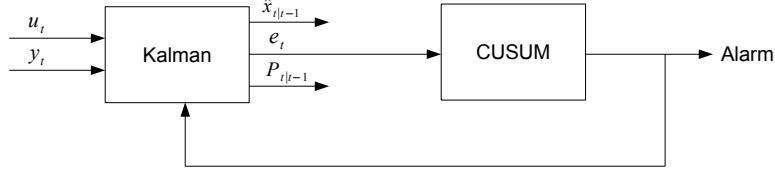


Figure 4.1. The change detector monitors the whiteness of the innovations, e_t from the KF.

another possible distance measure that could be used is

$$s_t = e_t^2. \quad (4.4)$$

Note that the innovations are squared in (4.4). This is done since it is detection of departure that is of interest and not manoeuvre.

Stopping Rule: The stopping rule, i.e., the algorithm that decides when the filter should be alarmed consists of two parts: First the distance measure is low pass filtered, here an averaging is used to calculate the test statistics l_t . Secondly this test variable is tried against a threshold to decide whether an alarm should go off or not. This is summarized in the CUSUM algorithm below. The stopping rule illustrated in Figure 4.2.

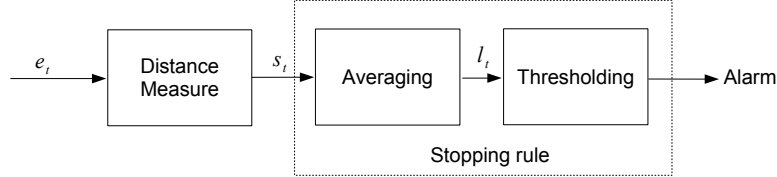


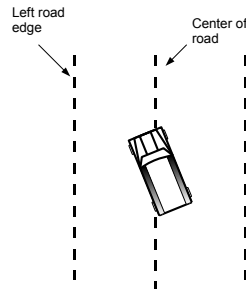
Figure 4.2. The change detector consists of a distance measure and a stopping rule.

Algorithm 3 CUSUM

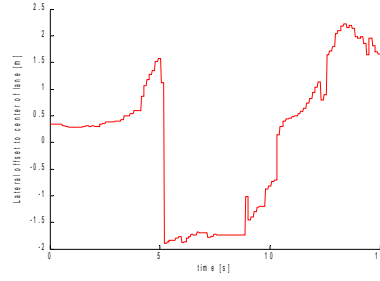
1. $l_t = l_{t-1} + s_t - \nu$.
 2. If $l_t > h$: Alarm, $l_t = 0$ and $t_{alarm} = t$.
 3. If $l_t < 0$: $l_t = 0$ and $\hat{t}_{change} = t$.
-

The test statistics l_t is a cumulative sum of the distance measure compensated for positive drifts via a drift term ν . Step 3 prevents negative drifts.

Lateral Offset: Since the LDWS has a unstable behavior when departing to the left on a highway caused by the road markings on left side of the road i.e., the LDWS measures the vehicle position relative the center of the left lane. The assumption is illustrated in Figure 4.3. However this is not as problematic as it might seem since the sudden drop in offset seen in Figure 4.3(b) can be detected by using some change detection method. In this Master's thesis, a CUSUM [8] is used to detect the change in lateral offset.



(a) Vehicle departing to the left.



(b) Lateral offset measurement.

Figure 4.3. LDWS measures the position in the left lane.

Chapter 5

Filter Evaluation

To evaluate the derived filter, tests with both simulated and experimental data were performed. In this chapter the results from these tests are presented.

5.1 Monte Carlo Simulations

A procedure to test the derived filter using M realizations of data y_t , is to use Monte Carlo simulations as follows: First, the following nonlinear time continuous model is solved using a Runge-Kutta method:

$$\dot{x}(t) = f(x(t)),$$

$$f(x(t)) = \begin{pmatrix} \frac{1}{J_z} \left(2C_f a \cos \delta \left(\delta - \arctan\left(\frac{v_y + l_f \dot{\Psi}}{v_x}\right) \right) - 2C_f l_r \left(\arctan\left(\frac{-v_y + l_r \dot{\Psi}}{v_x}\right) \right) \right) + \delta \frac{2l_f C_f}{J_z} \\ \frac{1}{m} \left(2C_f \cos \delta \left(\delta - \arctan\left(\frac{v_y + l_f \dot{\Psi}}{v_x}\right) \right) - 2C_r \left(\arctan\left(\frac{-v_y + l_r \dot{\Psi}}{v_x}\right) \right) \right) + \delta \frac{2C_f}{m} \\ c_1 v_x \\ 0 \\ \dot{\Psi} - (c_0 + c_1 l_f) v_x \\ v_x \sin(\theta) + v_y \cos(\theta) \\ v_x \sin(\theta) + v_y \cos(\theta) \\ 0 \\ 0 \end{pmatrix}, \quad (5.1)$$

where the input signals $\delta(t)$, $c_0(t)$ and $v_x(t)$ are specified to fit a given scenario. The continuous time solution is denoted $x(t)^{True}$ and the sampled x_t^{True} . Now the M realizations of data, denoted $y_t^{(j)}$, $j = 1, 2, \dots, M$, is generated from the measurement equation (3.51c) as

$$y_t = h(x_t^{True}) + e_t, \quad (5.2)$$

where e_t is Gaussian noise, unique for each realization. The derived Kalman filters are now applied on all the data sets, y_t^j , and the resulting estimates \hat{x}_t^j are compared to the true states, x_t^{True} , using the *root mean square error* (RMSE) [8] here defined as:

$$\text{RMSE}(t) = \left(\frac{1}{M} \sum_{j=1}^M \left\| x_t^{True} - \hat{x}_t^j \right\|_2^2 \right)^{\frac{1}{2}} \quad (5.3)$$

Note that the RMSE must be calculated for each sensor type individually otherwise signals with small amplitude could have a large error without affecting the RMSE.

5.2 Simulation Input Signals

In this section the different input signals needed to solve (5.1) are specified.

Vehicle Speed and Steering Wheel Angle: To simulate the vehicle speed measurement following function has been used:

$$v_x^{sim} = \Delta_{v_x} \cdot \left\lfloor \left(\frac{v_x^{True} + e_{t,v_x}}{\Delta_{v_x}} \right) \right\rfloor, \quad (5.4)$$

where

$$\Delta_{v_x} = 0.25 \text{ [km/h]}, \quad (5.5a)$$

$$\text{Cov}(e_{t,v_x}) = \sigma_{v_x}^2, \quad (5.5b)$$

and the $\lfloor \cdot \rfloor$ operator rounds downwards to the nearest integer. In Figure 5.1 a simulated signal and a measured signal are presented for comparison. The signal

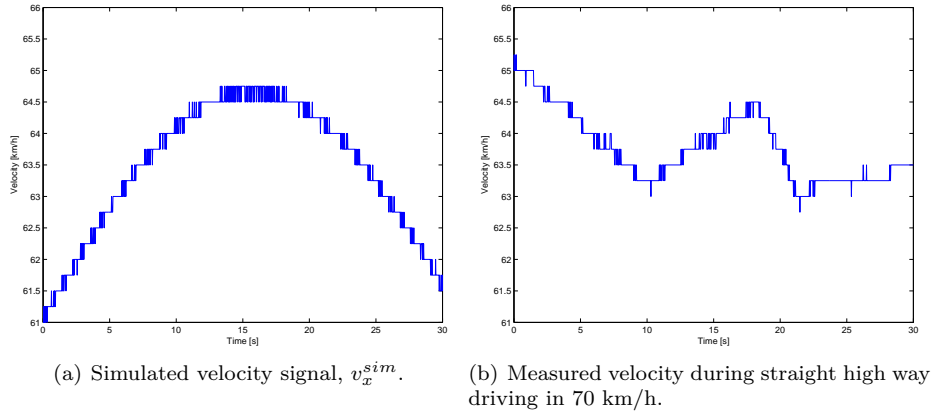


Figure 5.1. A comparison between a simulated velocity signal and measured velocity. Note that it is the noise that is of interest for comparison.

in Figure 5.1(a) has been created using (5.4) with

$$\sigma_{v_x}^2 = (2 \cdot 10^{-4})^2, \quad (5.6)$$

$$v_x^{True} = 17 + \sin(t/10)[m/s], \quad (5.7)$$

and the signal in Figure 5.1(b) has been recorded during straight highway driving in 70 km/h.

The steering wheel angle is harder to model since it is dependent on the driver, road structure, etc. Therefore the somewhat unrealistic assumption that the steering wheel angle is an almost noise free signal is made. The simulated steering angle is modeled as:

$$\delta^{sim} = \Delta_\delta \cdot [(\frac{\delta^{True} + e_{t,\delta}}{\Delta_\delta})], \quad (5.8)$$

where

$$\Delta_\delta = 0.1 [^\circ], \quad (5.9a)$$

$$Cov(e_{t,\delta}) \approx 0. \quad (5.9b)$$

It is important to notice that the steering wheel angle and the wheel turn angle are not the same. In [12] it is suggested that a steering wheel angle of 100° should correspond to a wheel turn angle of 0.1 rad when driving in 50 km/h. The signal in Figure 5.2 has been recorded during straight highway driving in 70 km/h.

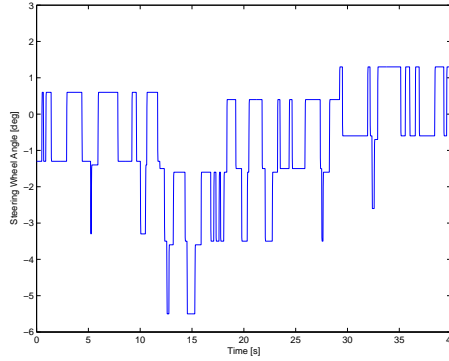


Figure 5.2. Measured steering wheel angle during straight highway driving in 70 km/h.

Road Curvature and Lane Width: In the two scenarios the road is modeled as either straight i.e., $c_0 = 0$ or as a curve with a constant curvature. According to [5], a Swedish 50 km/h road should normally not have any curves with a radius less than 140 meters. Therefore the curvature has been set to $\sigma_0 = 1/140$ in the fast curve entering simulation. The lane width is in all simulations assumed to be constantly 4 meters, i.e., $W = 4$.

5.3 Simulation Scenarios

Two different scenarios have been simulated to test the performance of the estimators. Both simulations use the measurement noise levels given in Table 5.1. The noise levels are chosen so that they are of the same order as the noise levels on the experimental data.

Table 5.1. Measurement noise variance added to the true states in the simulation

Measurement	Noise Variance
Yaw rate, $\dot{\Psi}^m$	0.035^2
Curvature, c_0^m	0.000063^2
Lateral offset, y_{off}	0.01^2
Lateral acceleration, a_y	0.2^2

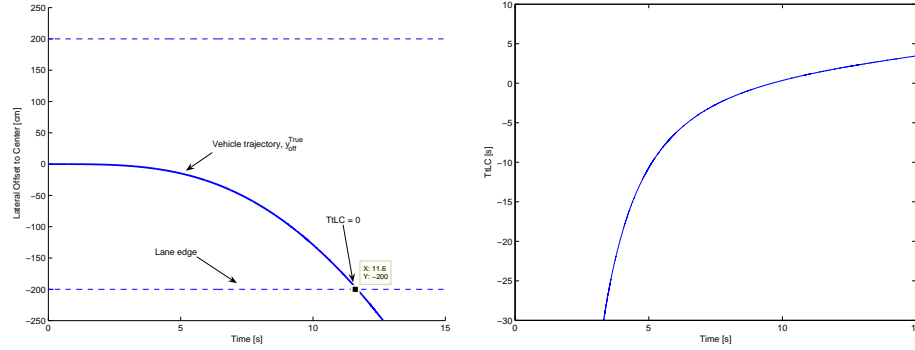
Unintentional Lane Departure: The simulated scenario used in this section is described in Figure 5.3. The trajectory in Figure 5.3 represents a vehicle slowly drifting to the right of the road until it finally departs after 11.6 seconds. In Table 5.2 the signals used in the scenario are specified. Using these signals and $x_0 = (0 \ 0 \ 0 \ 0 \ 0 \ 0 \ 14 \ 0)^T$ as initial state vector, 500 data sets of measurements are generated.

Table 5.2. Signals used in drift simulation

Measurement	Signal Definition
Longitudinal Velocity	$v_x^{True} = 14 + \sin(2\pi t/20) [m/s]$
Wheel Turn Angle	$\delta_w^{True} = -0.001 \cdot \sin(2\pi t/80) [rad]$
Road Curvature	$\sigma_0 = 0 [1/m]$
Lane Width	$W = 4 [m]$

The initial state vectors x_0^{KF} and x_0^{EKF} , process noise Q^{KF} and Q^{EKF} , and initial state error matrix P_0 are

$$\begin{aligned}
x_0^{KF} &= (0 \ 0 \ 0 \ 0 \ 0 \ 0 \ 2 \ 0 \ 0)^T, \\
x_0^{EKF} &= (0 \ 0 \ 0 \ 0 \ 0 \ 0 \ 2 \ 14 \ 0 \ 0 \ 0)^T, \\
Q^{KF} &= \text{diag}((10^{-3})^2 \ (10^{-3})^2 \ (10^{-7})^2), \\
Q^{EKF} &= \text{diag}((10^{-3})^2 \ (10^{-3})^2 \ (10^{-7})^2 \ 0.05^2 \ 0.01^2), \\
P_0^{KF} &= \text{diag}(1^2 \ 10^2 \ 10^2 \ 1^2 \ 10^2 \ 10^2 \ 10^2 \ 1^2 \ 1^2 \ 1^2), \\
P_0^{EKF} &= \text{diag}(1^2 \ 10^2 \ 10^2 \ 1^2 \ 10^2 \ 10^2 \ 10^2 \ 1^2 \ 1^2 \ 1^2 \ 1^2),
\end{aligned}$$



(a) The drift scenario is generated using the signals in Table 5.2.

(b) The true TtLC.

Figure 5.3. Vehicle trajectory and corresponding TtLC.

Table 5.3. RMSE analysis using 500 Monte Carlo runs.

Estimation	KF	EKF
Lateral pos., $y_{off,c}$ [m]	0.0866	0.0992
Heading, θ [deg]	0.6073	0.6131
Lateral Velocity, v_y [m/s]	0.0114	0.0132
Yaw Rate, Ψ [deg/s]	0.1662	0.1833
Curvature c_0 [1/m]	0.0009	0.0008
Clothid parameter c_1 [1/m ²]	0.0002	0.0002

where $\text{diag}(x_1, \dots, x_n)$ is a diagonal matrix with x_1, \dots, x_n as the diagonal. In Table 5.3 we see that both filters perform well for the given scenario. The TtLC has not been evaluated using RMSE, since when the heading angle is small the estimated heading starts to switch sign and the RMSE quickly becomes very large. In Figure 5.4 the true and the estimated TtLC from a single run is plotted. From Figure 5.4 it should be noticed that the TtLC estimation improves as the heading angle grows, which indicates that the most difficult cases for the filter to handle is when the vehicle hugs the lane. It should also be noticed that even though the TtLC estimation seems poor a potential warning would still be correct if the alarm threshold is set to 1 second.

Fast Curve Entering: The scenario simulated in this section uses a road with constant curvature, $c_0 = \frac{1}{R} = \frac{1}{140}$. In Figure 5.5, a road section is plotted together with the trajectory of a vehicle departing from the road.

The input signals presented in Table 5.4 differs only slightly from the ones used in section 5.3.

The initial state vectors x_0^{KF} and x_0^{EKF} , process noise Q^{KF} and Q^{EKF} , and

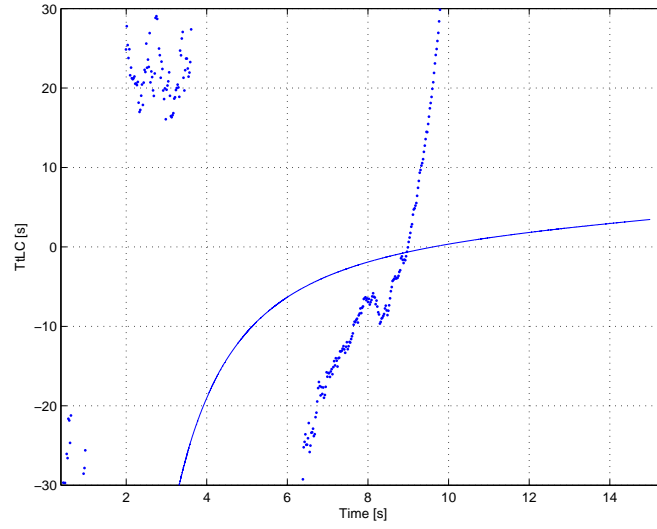


Figure 5.4. Estimated (dots) and true (solid line) TtLC. The picture shows that the estimated TtLC becomes more and more inaccurate as it increases.

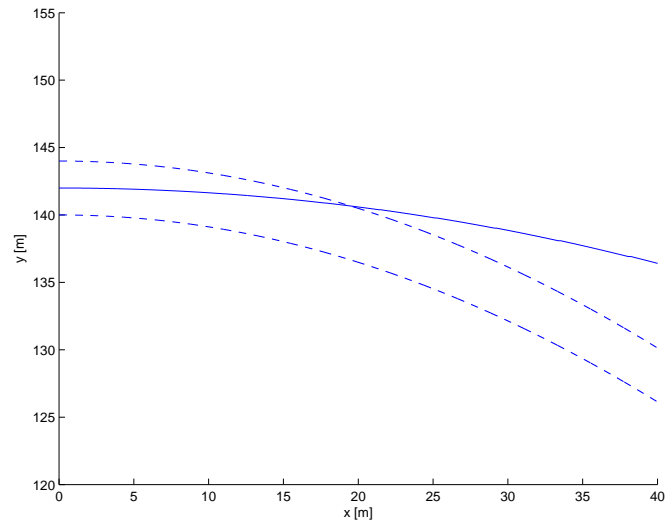


Figure 5.5. The dashed lines represent a road with constant curvature $c_0 = \frac{1}{140}$ and the solid line is the trajectory of a vehicle departing due to a too small steering angle.

Table 5.4. Signals used in fast curve entering simulation

Measurement	Signal Definition
Longitudinal Velocity	$v_x^{True} = 14 + \sin(2\pi t/20) [m/s]$
Wheel Turn Angle	$\delta_w^{True} = -0.01 \cdot \sin(2\pi t/80) [rad]$
Road Curvature	$\sigma_0 = 1/140 [1/m]$
Lane Width	$W = 4 [m]$

initial state error matrix P_0 are

$$\begin{aligned}
x_0^{KF} &= (0 \ 0 \ 0 \ 0 \ 0 \ 0 \ 2 \ 0 \ 0)^T, \\
x_0^{EKF} &= (0 \ 0 \ 0 \ 0 \ 0 \ 0 \ 2 \ 14 \ 0 \ 0 \ 0)^T, \\
Q^{KF} &= \text{diag}((10^{-3})^2 \ (10^{-3})^2 \ (10^{-7})^2), \\
Q^{EKF} &= \text{diag}((10^{-3})^2 \ (10^{-3})^2 \ (10^{-7})^2 \ 0.05^2 \ 0.01^2), \\
P_0^{KF} &= \text{diag}(1^2 \ 10^2 \ 10^2 \ 1^2 \ 10^2 \ 10^2 \ 10^2 \ 1^2 \ 1^2 \ 1^2), \\
P_0^{EKF} &= \text{diag}(1^2 \ 10^2 \ 10^2 \ 1^2 \ 10^2 \ 10^2 \ 10^2 \ 1^2 \ 1^2 \ 1^2 \ 1^2).
\end{aligned}$$

Table 5.5. RMSE analysis using 500 Monte Carlo runs

Estimation	KF	EKF
Lateral pos., $y_{off,c}$ [m]	0.2201	0.1245
Heading, θ [deg]	2.8877	0.6417
Lateral Velocity, v_y [m/s]	0.0153	0.0273
Yaw Rate, Ψ [deg/s]	0.1031	0.2578
Curvature c_0 [1/m]	0.0011	0.0008
Clothid parameter c_1 [1/m ²]	0.0003	0.0003

From the results in Table 5.5 we see that the lateral position and the heading angle are clearly better estimated by the extended Kalman filter. The conclusion must therefore be that the EKF is a better choice when tracking strong manoeuvres. To summarize, the simulations show that the filter has potential to function well, but deeper analysis on experimental data is needed since there are many simplifications done in the simulations.

5.4 Experiments

The evaluation using experimental data is done for the EKF implementation. This decision was taken since the EKF provides the possibility to filter the steering wheel angle and the vehicle speed and since the KF has not proved significantly better in the simulations. The preformed test drives are categorized into:

1. No Warnings, the vehicle is driven so that the camera system generates no warnings.
2. Unintentional Lane Departure Right/Left, the vehicle is driven on a straight highway and forced to slowly depart from the lane to the right/left.
3. Fast Unintentional Lane Departure Right/Left, the vehicle is forced to depart quickly from the lane.
4. Lane Hugging, the vehicle is driven closely to lane edge but without departing.

The goal of this testing is to find a level on the TtLC that can be used as lower threshold for warning the driver. Also it will be investigated whether a CUSUM-test can improve the detection of fast lane departures.

Following parameters are used throughout in the experiments. The initial state vector x_0^{EKF} , process noise Q^{EKF} , measurement noise R^{EKF} , and initial state error matrix P_0 are

$$\begin{aligned}
 x_0^{EKF} &= (0 \ 0 \ 0 \ 0 \ 0 \ 0 \ 2 \ 14 \ 0 \ 0 \ 0)^T, \\
 Q^{EKF} &= \text{diag}((10^{-2})^2 \ (10^{-2})^2 \ (10^{-5})^2 \ 0.05^2 \ 0.001^2), \\
 R^{EKF} &= \text{diag}((0.035)^2 \ (10^{-13})^2 \ (0.05)^2 \ (0.05)^2 \ (0.02)^2 \ (0.00005)^2 \ (0.2)^2), \\
 P_0^{EKF} &= \text{diag}(1^2 \ 1^2 \ 1^2 \ 1^2 \ 1^2 \ 1^2 \ 1^2 \ 1^2 \ 1^2 \ 1^2 \ 1^2).
 \end{aligned}$$

Notice that this is not the same as in the simulations. For example the steering angle is made slower i.e., its process noise is smaller and the yaw rate is faster.

No Warnings: To find an upper threshold, the car has been driven during normal conditions when the camera based system produced no warnings. During this kind of driving the TtLC should always exceed some value which will be taken as an upper threshold. In Figure 5.6, the TtLC during normal highway driving, estimated by the EKF, is plotted. Note that the sign on the TtLC corresponds to the sign of the heading angle, i.e., if the vehicle departs to the right the TtLC should be estimated to a smaller and smaller negative value. In Table 5.6 the lowest TtLC that was estimated during normal highway driving is presented.

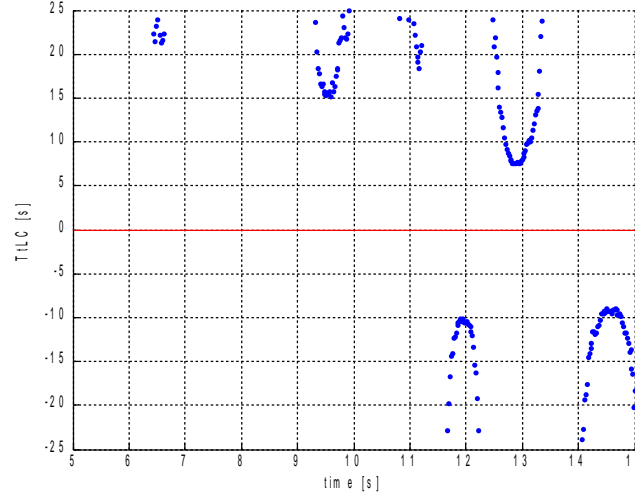


Figure 5.6. TtLC during normal highway driving in 100 km/h. Negative TtLC means that the heading of the vehicle is negative, i.e., heading to the right.

Table 5.6. Upper threshold on TtLC

Velocity	TtLC [s], EKF
80	2.50
90	1.96
100	1.51
110	1.21

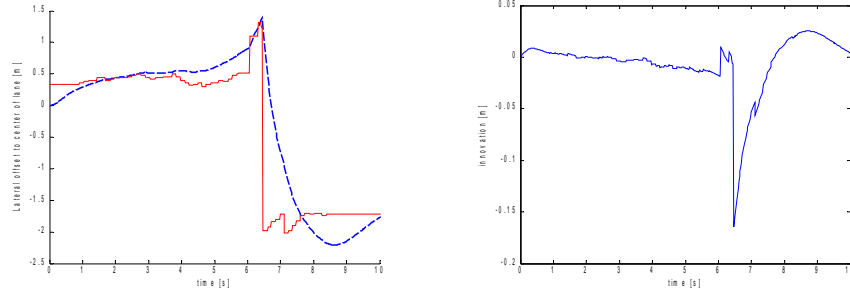
Unintentional Lane Departure Right: To find a lower threshold on the TtLC, the filter is tested on data when the vehicle drifts right. The filter is compared to the camera. In Table 5.7 the value on TtLC, that the filter estimated when the LDWS produced a correct warning is presented. Note that the sign on the TtLC only comes from whether the heading angle is positive or negative. When the vehicle departs to the right the heading angle should be negative, see Figure 3.3.3 for the definition of the states. It is also presented in Table 5.7 how much earlier the filter warns if the lower threshold is put to 0.5 seconds denoted δt . The comment column contains a remark when the camera based LDWS failed to produce a warning, i.e., there is no reference to compare the TtLC estimation with.

Unintentional Lane Departure Left: In this section a lane departure to the left is presented. Drift to the left is more problematic than to the right, since the LDWS has to decide when to start measuring the position to the left. In this

Table 5.7. Estimated TtLC and Δt .

Velocity	TtLC [s], EKF	Δt	Comment
80	-0.666	1.31	LDWS fails.
	-0.473	1.72	
	-0.624	1.02	
	-	-	
90	-0.249	1.41	LDWS fails.
	-0.758	0.27	
	-	-	
	-0.530	0.27	
100	-0.364	1.95	LDWS fails.
	-0.311	3.49	
	-0.250	3.10	
	-	-	
110	-	-	LDWS fails.
	-	-	LDWS fails.
	-	-	LDWS fails.
	-0.288	0.7	
	-0.016	3	
	-	-	

Master's thesis , the suggested solution to this problem is to use a CUSUM-test together with the TtLC decision strategy. Why Drift to the left is problematic is illustrated in Figure 5.7



(a) Measured (solid) and estimated (dashed) lateral offset.

(b) Innovations of the lateral offset.

Figure 5.7. Drift to the left, the camera loses track of the lane markings as the vehicle departs from the lane.

Fast Unintentional Lane Departure: A fast drift situation is much better managed by the fused system in comparison to the camera based system since

when the camera experience a rapid lateral movement it loses track of the lane. However, since this situation is not detected by the camera, there is no reference to compare with i.e., it is not possible to measure whether the estimated TtLC is correct or not. It is therefore assumed that the yaw rate measurement detects all large lateral manoeuvre, hence it can be used to verify that there are no false alarms. Under these assumptions the testing has been performed on a straight highway the results are presented in Table 5.8 and Table 5.9.

Table 5.8. Fast drift right. At each velocity five lane departures were conducted except for 90 km/h, where only three departures were conducted

Velocity	No. warnings, LDWS	No. of warnings, EKF
60	0	5
70	0	5
80	1	5
90	1	3
100	0	5
110	0	5

Table 5.9. Fast drift left, at each velocity five lane departures were conducted

Velocity	No. warnings from LDWS	No. of warnings, EKF
60	1	5
70	0	5
80	0	5
90	0	5
100	0	5
110	1	5

Lane hugging: Lane hugging is the situation when the driver approaches the lane edge with small heading angle without departing from the lane. After several tests were performed it must be concluded that the suggested system does not improve the performance of the LDWS in this situation, at least not without another more suitable decision strategy. In Table 5.10 the results from testing lane hugging are presented. With a threshold on 0.5 seconds, the filter will manage well in low velocities, but in normal highway velocities above 100 km/h, it starts generating false alarms.

CUSUM-test: The CUSUM-test has after much testing using the experimental data been found hard to use for slow lane departures since the innovations mostly are quite small. For fast lane departures, where the innovations often are bigger, it is more likely to get correct warnings from a CUSUM-test. From Table 5.8 and 5.9 it is clear that there are very little data available to use as reference, since

Table 5.10. Lane hugging No. of false alarms

Velocity	No. off false alarms, LDWS	No. off false alarms, EKF
70	0	0
90	0	0
110	1	3

the camera based LDWS generates few correct warnings when the innovations are large. The suggested use of the CUSUM-test is therefore to use it together with the TtLC estimation, i.e., if the test generates a warning and the TtLC estimation at the same time is small, less false warnings should be generated. The tuning of the CUSUM parameters ν and h , i.e., the drift compensation and the alarm level, is therefore the tuning parameters are chosen rather conservative to avoid false warnings. In Figure 5.8 the yaw rate, the TtLC and the warnings from a CUSUM-test using data recorded during a fast lane departure is plotted. The yaw rate tells us that the vehicle was departing to the right, starting around 3 seconds and then after another 1 second we see that the yaw rate starts to increase again i.e., the driver tries to correct the unintentional lane departure. Ideally the warning should therefore come just before 4 seconds.

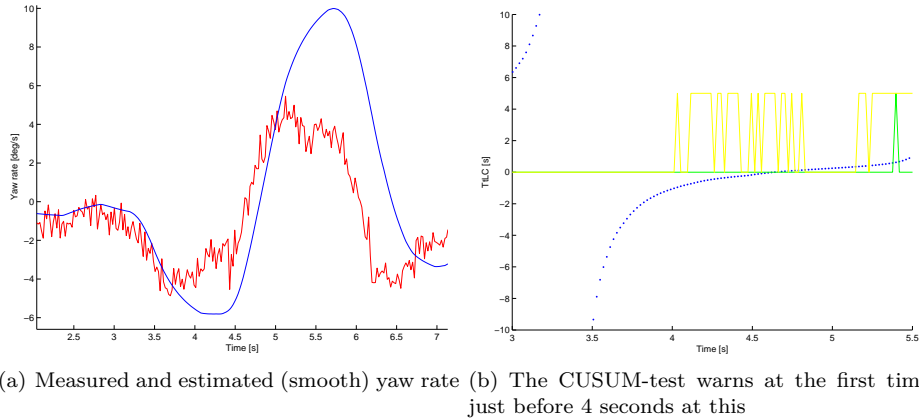


Figure 5.8. TtLC estimation (dotted) with CUSUM-test warnings (solid). The data was recorded in 110 km/h performing a fast lane departure to the right.

Chapter 6

Conclusions and Future Work

6.1 Results

Positioning: This Master's thesis has proposed and evaluated a model for enhanced lane departure warning. The goal has been to achieve a system that handles the situations where a camera based LDWS fails. The increase in functionality has been achieved using an IMU to estimate the vehicle lateral position. The most important aspect of the positioning problem is to estimate the vehicle heading angle correctly, which, if the camera measurements fails, dominates the positioning error.

Time to Lane Crossing: The decision strategy, TtLC, that is used in this Master's thesis has proved to be a robust method for detecting lane departures. However, it is a bit inaccurate as the velocity grows and the lateral offset is small. This is, however, a generally difficult problem since the real TtLC actually does decrease when the velocity is high.

Accident Types: Fast curve entering cannot be improved by the SF model that has been suggested in this Master's thesis, since this demands more knowledge of the road which an internal measurement unit cannot provide. The fused lane departure warning system is made less sensitive to rapid movements and in most cases a better warning is produced. Fast unintentional lane departure is the accident type that really is improved by the fused system, mainly since the camera fails to produce reliable readings in this situation and the IMU has a smaller signal-to-noise ratio, here improving the heading estimation.

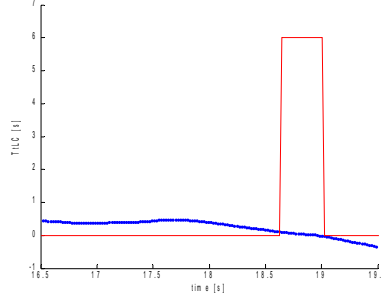


Figure 6.1. The vehicle is hugging the lane resulting in a small TtLC (thick line). The pulse represents the warning that the camera system provided in this situation.

6.2 Future Work

There are many interesting aspects that deserve further investigation.

Curvature estimation: The filter is very poor at handling the curvature, which has to do with the camera measurements which are unreliable, and tend to disturb the filter rather than improving it. Therefore as future work an evaluation of the usage of the curvature more as a signal for improved decision making than as a measurement is suggested.

Discretization: The discretization method used in this Master's thesis is the simplest there is, and there are much more refined methods such as e.g., Tustin's formula [9]. Therefore an investigation of the error that originates from the discretization is suggested as future work.

Lane Hugging: When analyzing the data, several situations were found when the estimated TtLC were small for several seconds before the warning should come. This situation is presented in Figure 6.1 and typical arises when the velocity is large and the lateral offset relative small. One way to approach this situation could be to analyze the derivative of the TtLC. A small derivative could perhaps be used interpreted as a less dangerous situation than the TtLC alone would imply.

Jerk: In [8] it is pointed out that many filters can improve their tracking capability by introducing acceleration as a state and assuming that the process noise represents the change in acceleration, i.e., jerk. A comparison of how much this actually improves the filter derived in this Master's thesis would be very interesting.

Bibliography

- [1] B. D. O. Andersson and J. M. Moore. *Optimal Filtering*. Prentice-Hall, Inc., Englewood Cliffs, N.J., 1979.
- [2] Y. Bar-Shalom and T. E. Fortmann. *Tracking and Data Association*. Academic Press, Inc., 1988.
- [3] Y. Bar-Shalom and X. Li. *Estimation and Tracking: Principles, Techniques and Software*. Artech House, 1993.
- [4] E. D. Dickmanns and B. D. Mysliwetz. Recursive 3-D Road and Relative Ego-State Recognition. *IEEE Transactions on Pattern Analysis and Machine Intelligence*, 14:199–213, 1992.
- [5] A. Eidehall. An Automotive Lane Guidance System. Technical Report Licentiate Thesis no. 1122, Department of Electrical Engineering, Linköping University, SE-581 83 Linköping, Sweden, Nov 2004.
- [6] W. Elmenreich. An Introduction to Sensor Fusion. Technical report, Vienna University of Technology, Nov 2002.
- [7] M. Grewal and Andrews A. *Kalman Filtering Theory and Practice Using MATLAB*. John Wiley and Sons, 2 edition, 2001.
- [8] F. Gustafsson. *Adaptive Filtering and Change Detection*. John Wiley and Sons, 2000.
- [9] F. Gustafsson, L. Ljung, and M. Millnert. *Signalbehandling*. Studentlitteratur, 2000.
- [10] T Kailath, A. H. Sayed, and B. Hassibi. *Linear Estimation*. Prentice Hall, 2000.
- [11] Rickard Karlsson. *Particle Filtering for Positioning and Tracking Applications*. PhD thesis, Mar 2005.
- [12] U. Kiencke and L. Nielsen. *Automotive Control Systems For Engine, Driveline and Vehicle*. Springer Verlag, 2 edition, 2005.
- [13] L. Nielsen and L. Eriksson. *Course material, Vehicular Systems*. ISY Linköping Institute of Technology, 2005.

-
- [14] E. Ryding and E. Öhlund. Lane Keeping Aid - a driver support system for cars. Master's thesis, ISY Linköping Institute of Technology, April 2002. LITH-ISK-EX-3207-2002.
 - [15] Thomas Schön. *Estimation of Nonlinear Dynamic Systems - Theory and Applications*. PhD thesis, Linköping, Sweden, Feb 2006.
 - [16] W. van Winsum, K.A. Brookhuis, and D. de Waard. A comparison of different ways to approximate time-to-line crossing (TLC) during car driving. In *Accident Analysis and Prevention 32*, pages 47–56, April 1999.

Chapter 7

Appendix

Discretized Kalman filter

Here the discretized KF is presented, the discretization is done using backwards difference.

$$x_t = \begin{pmatrix} x_1 \\ x_2 \\ x_3 \\ x_4 \\ x_5 \\ x_6 \\ x_7 \end{pmatrix} = \begin{pmatrix} \dot{\Psi} \\ v_y \\ c_0 \\ c_1 \\ \theta \\ y_{off,c} \\ y_{off,re} \end{pmatrix}, \quad (7.1a)$$

$$F_t(v_x) = \begin{pmatrix} 1 + T_s a_{11} & T_s a_{12} & 0 & 0 & 0 & 0 & 0 \\ T_s a_{21} & 1 + T_s a_{22} & 0 & 0 & 0 & 0 & 0 \\ 0 & 0 & 1 & T_s v_x & 0 & 0 & 0 \\ 0 & 0 & 0 & 1 & 0 & 0 & 0 \\ T_s & 0 & -T_s v_x & 0 & 1 & 0 & 0 \\ 0 & T_s & 0 & 0 & T_s v_x & 1 & 0 \\ 0 & T_s & 0 & 0 & T_s v_x & 0 & 1 \end{pmatrix}, \quad (7.1b)$$

$$G_{u,t} = \begin{pmatrix} T_s b_1 \\ T_s b_2 \\ 0 \\ 0 \\ 0 \\ 0 \\ 0 \end{pmatrix} \quad (7.1c)$$

Upphovsrätt

Detta dokument hålls tillgängligt på Internet — eller dess framtida ersättare — under 25 år från publiceringsdatum under förutsättning att inga extraordinära omständigheter uppstår.

Tillgång till dokumentet innebär tillstånd för var och en att läsa, ladda ner, skriva ut enstaka kopior för enskilt bruk och att använda det oförändrat för icke-kommersiell forskning och för undervisning. Överföring av upphovsrätten vid en senare tidpunkt kan inte upphäva detta tillstånd. All annan användning av dokumentet kräver upphovsmannens medgivande. För att garantera äktheten, säkerheten och tillgängligheten finns det lösningar av teknisk och administrativ art.

Upphovsmannens ideella rätt innefattar rätt att bli nämnd som upphovsman i den omfattning som god sed kräver vid användning av dokumentet på ovan beskrivna sätt samt skydd mot att dokumentet ändras eller presenteras i sådan form eller i sådant sammanhang som är kränkande för upphovsmannens litterära eller konstnärliga anseende eller egenart.

För ytterligare information om Linköping University Electronic Press se förlagets hemsida <http://www.ep.liu.se/>

Copyright

The publishers will keep this document online on the Internet — or its possible replacement — for a period of 25 years from the date of publication barring exceptional circumstances.

The online availability of the document implies a permanent permission for anyone to read, to download, to print out single copies for your own use and to use it unchanged for any non-commercial research and educational purpose. Subsequent transfers of copyright cannot revoke this permission. All other uses of the document are conditional on the consent of the copyright owner. The publisher has taken technical and administrative measures to assure authenticity, security and accessibility.

According to intellectual property law the author has the right to be mentioned when his/her work is accessed as described above and to be protected against infringement.

For additional information about the Linköping University Electronic Press and its procedures for publication and for assurance of document integrity, please refer to its www home page: <http://www.ep.liu.se/>